Appl. Numer. Math. 206 (2024) 29–47

Contents lists available at ScienceDirect

Applied Numerical Mathematics

journal homepage: www.elsevier.com/locate/apnum

Research Paper

The virtual element method for a contact problem with wear and unilateral constraint

Bangmin Wu [a], Fei Wang [b,*], Weimin Han [c]

[a] College of Mathematics and Systems Science, Xinjiang University, Urumqi, 830046, Xinjiang, China
[b] School of Mathematics and Statistics, Xi'an Jiaotong University, Xi'an, Shaanxi 710049, China
[c] Department of Mathematics, University of Iowa, Iowa City, IA 52242, USA

ARTICLE INFO

MSC:
65N30
49J40

Keywords:
Frictional contact
Wear
Quasi-variational inequality
Virtual element method
Error estimates

ABSTRACT

This paper is dedicated to the numerical solution of a mathematical model that describes frictional quasistatic contact between an elastic body and a moving foundation, with the wear effect on the contact interface of the moving foundation due to friction. The mathematical problem is a system consisting of a time-dependent quasi-variational inequality and an integral equation. The numerical method is based on the use of the virtual element method (VEM) for the spatial discretization of the variational inequality and a variable step-size left rectangle integration formula for the integral equation. The existence and uniqueness of a numerical solution are shown, and optimal order error estimates are derived for both the displacement and the wear function for the lowest order VEM. Numerical results are presented to demonstrate the efficiency of the method and to illustrate the numerical convergence orders.

1. Introduction

The process of frictional contact between deformable bodies or between a deformable body and a rigid foundation is common in a wide variety of applications. Contact problems are usually studied in the framework of variational or hemivariational inequalities, which have garnered significant attention from numerous researchers. In this paper, we consider the numerical solution of a contact problem involving wear and unilateral constraint. The weak formulation of the problem is a system consisting of a time-dependent quasi-variational inequality and an integral equation. Numerical methods are needed to solve such a problem. The finite element method has been employed to solve quasi-variational inequalities, and a priori error estimates have been derived in a number of papers, such as [20,21,26]. In [38], several discontinuous Galerkin methods with linear elements are introduced for solving a frictional contact problem with normal compliance, and a priori error estimates are established in [33].

In recent years, as an extension of the classical finite element method, the virtual element method (VEM) has gained popularity since it was first introduced in 2013 ([3]). The VEM has advantages in handling general (including non-convex) polygonal elements, making it easier to solve problems with complex geometries. By introducing the projection operator from a virtual element space to a polynomial space, the stiffness matrix can be formed without actually computing the non-polynomial functions. The VEM has been applied to solve a variety of scientific and engineering problems (e.g., [1,2,6,17,27,39]). In particular, it has been utilized to solve variational and hemivariational inequalities. The virtual element method is applied to solve a two-body contact problem in [31]

* Corresponding author.
E-mail addresses: bmwu_math@xju.edu.cn (B. Wu), feiwang.xjtu@xjtu.edu.cn (F. Wang), weimin-han@uiowa.edu (W. Han).

https://doi.org/10.1016/j.apnum.2024.08.004
Received 25 January 2024; Received in revised form 27 May 2024; Accepted 2 August 2024

Available online 6 August 2024

without an error estimate. Remarkably, even when the initial meshes for the two subdomains do not align, the inherent capability of VEM allows for seamless insertion of new nodes along the contact interface. Consequently, the initially non-matching meshes undergo transformation into compatible meshes, thereby highlighting a distinctive advantage of VEM over FEM. For the numerical analysis of the VEM for two-body contact problems, optimal error estimates are derived in [32] for both frictionless and frictional contact cases. In [34,35], a priori error estimates of VEM are established for solving the obstacle problem and simplified friction problem, respectively. The VEM is studied for a frictional contact problem in [13]. In [14,36], the VEM is developed and analyzed for solving elliptic hemivariational inequalities with applications to contact mechanics. In [37], the virtual element method was employed to solve a frictional contact problem with normal compliance and Coulomb's law of dry friction.

Since the contact process may cause material wear or even damage, wear effects have been taken into account in studies of various contact problems, cf. [8,16,21,25,30]. In [29], a mathematical model is proposed and studied for contact with wear described by Archard's law of surface wear. In this model, the friction between a deformable body and a foundation leads to wear on the contact surface of the foundation. Well-posedness of the problem is also provided in [29]. A numerical approximation of this model is studied in [24], where error bounds are derived for a fully discrete scheme. A more general fully discrete scheme with the finite element method is given in [19], which allows for an arbitrary partition of the time interval, and optimal order error estimates are derived. In this paper, we investigate the virtual element method for solving the contact problem incorporating the wear effect, which can be represented by a time-dependent quasi-variational inequality accompanied by an integral equation. The existence and uniqueness of the numerical solution are obtained for the fully discrete scheme. Furthermore, we derive optimal-order error estimates for numerical solutions of both the displacement and the wear function with the lowest order VEM.

The rest of this paper is structured as follows. In Section 2, we introduce the contact problem with wear and its weak formulation. In Section 3, we develop a numerical method using the virtual element method (VEM) for the spatial discretization and a variable step-size left rectangle integration formula for the integral equation. In Section 4, we derive optimal-order error estimates for both the displacement and the wear function. In Section 5, computer simulation results are reported to provide numerical evidence of the theoretically predicted convergence orders.

2. Contact problem with wear and its weak formulation

Let $\Omega \subset \mathbb{R}^d$ $(d = 2, 3)$ denote the configuration of a deformable elastic body under the action of a volume force of density $\boldsymbol{f}_1$. Denote by "$\cdot$" and "$\|\cdot\|$" the scalar product and Euclidean norm in $\mathbb{R}^d$. We assume Ω is an open bounded connected domain with a Lipschitz boundary Γ, which is partitioned into three disjoint measurable components: Γ_D, Γ_N and Γ_C, where $\text{meas}(\Gamma_D) > 0$. The body is clamped on Γ_D, so the displacement is equal to $\mathbf{0}$ on Γ_D. A surface traction of density $\boldsymbol{f}_2$ is exerted on the boundary Γ_N.

The displacement $\boldsymbol{u} : \Omega \subset \mathbb{R}^d \to \mathbb{R}^d$ is a vector-valued function. The linearized strain tensor is defined as $\boldsymbol{\varepsilon}(\boldsymbol{u}) = \frac{1}{2}(\nabla \boldsymbol{u} + (\nabla \boldsymbol{u})^T)$. The symbol $\mathbb{S}^d$ denotes the space of 2nd-order symmetric tensors on $\mathbb{R}^d$ with the inner product given by $\boldsymbol{\sigma} : \boldsymbol{\tau} = \sigma_{ij}\tau_{ij}$. Throughout this paper, we adopt the summation convention over repeated indices, e.g., $\sigma_{ij}\tau_{ij}$ stands for $\sum_{i,j=1}^d \sigma_{ij}\tau_{ij}$. Let $\boldsymbol{\nu}$ be the unit outward normal to the boundary surface Γ. For a vector field $\boldsymbol{v}$ defined on the boundary, its normal component and tangential component $v_\nu = \boldsymbol{v} \cdot \boldsymbol{\nu}$ and $\boldsymbol{v}_\tau = \boldsymbol{v} - v_\nu \boldsymbol{\nu}$, respectively. Similarly, for a tensor-valued function $\boldsymbol{\sigma}$ defined on the boundary, its normal component is $\sigma_\nu = (\boldsymbol{\sigma}\boldsymbol{\nu}) \cdot \boldsymbol{\nu}$, while its tangential component is $\boldsymbol{\sigma}_\tau = \boldsymbol{\sigma}\boldsymbol{\nu} - \sigma_\nu \boldsymbol{\nu}$. For a tensor-valued function $\boldsymbol{\sigma}$, define its divergence by $\text{div}\,\boldsymbol{\sigma} = (\partial_j \sigma_{ij})_{1 \le i \le d}$. For any smooth symmetric tensor field $\boldsymbol{\sigma}$ and any smooth vector field $\boldsymbol{v}$, we have the following integration by parts formula:

$$\int_\Omega \text{div}\boldsymbol{\sigma} \cdot \boldsymbol{v}\, dx = \int_\Gamma \boldsymbol{\sigma}\boldsymbol{\nu} \cdot \boldsymbol{v}\, ds - \int_\Omega \boldsymbol{\sigma} : \boldsymbol{\varepsilon}(\boldsymbol{v})\, dx. \tag{2.1}$$

Following [29], we assume that the acceleration of the body is negligible and so the problem is quasi-static. In this model, the framework of the small strain theory is employed. We assume that the elastic body is in contact on Γ_C with a moving foundation made of a hard perfectly rigid material that is covered by a layer of soft material. The soft layer is deformable, so the elastic body may penetrate it. We consider the displacement of the body and the wear of the soft layer in a time interval $[0, T]$, $T > 0$.

Let

$$\boldsymbol{n}^*(t) = -\boldsymbol{v}^*(t)/\|\boldsymbol{v}^*(t)\|, \quad \alpha(t) = \kappa\|\boldsymbol{v}^*(t)\|, \tag{2.2}$$

where $\boldsymbol{v}^*(t) \neq \mathbf{0}$ denotes the velocity of the foundation and κ represents the wear coefficient. Here, for simplicity, we do not indicate explicitly the dependence of various functions on the spatial variable $\boldsymbol{x}$. This convention is commonly adopted in the literature in the area of contact mechanics and it will be systematically used throughout the remainder of this paper.

The classical formulation of the considered model is as follows.

Problem 2.1. *Find a stress field* $\boldsymbol{\sigma} : \Omega \times [0, T] \to \mathbb{S}^d$, *a displacement field* $\boldsymbol{u} : \Omega \times [0, T] \to \mathbb{R}^d$ *and a wear function* $w : \Gamma_C \times [0, T] \to \mathbb{R}_+ = [0, \infty)$ *such that for all* $t \in [0, T]$,

$$\boldsymbol{\sigma}(t) = \mathcal{C}\boldsymbol{\varepsilon}(\boldsymbol{u}(t)) \qquad \textit{in } \Omega, \tag{2.3}$$

$$-\text{div}\,\boldsymbol{\sigma}(t) = \boldsymbol{f}_1(t) \qquad \textit{in } \Omega, \tag{2.4}$$

$$\boldsymbol{u}(t) = \boldsymbol{0} \qquad \text{on } \Gamma_D, \tag{2.5}$$

$$\boldsymbol{\sigma}(t)\boldsymbol{\nu} = \boldsymbol{f}_2(t) \qquad \text{on } \Gamma_N, \tag{2.6}$$

$$\left.\begin{array}{l} u_\nu(t) \le g,\ \sigma_\nu(t) + p\left(u_\nu(t) - w(t)\right) \le 0, \\ (u_\nu(t) - g)\left(\sigma_\nu(t) + p(u_\nu(t) - w(t))\right) = 0 \end{array}\right\} \qquad \text{on } \Gamma_C, \tag{2.7}$$

$$-\boldsymbol{\sigma}_\tau(t) = \mu\, p(u_\nu(t) - w(t))\, \boldsymbol{n}^*(t) \qquad \text{on } \Gamma_C, \tag{2.8}$$

$$w'(t) = \alpha(t)\, p(u_\nu(t) - w(t)) \qquad \text{on } \Gamma_C, \tag{2.9}$$

$$w(0) = 0 \qquad \text{on } \Gamma_C. \tag{2.10}$$

Here, the constitutive law with an elasticity operator $\mathcal{C}$ is represented by (2.3), while (2.4) denotes the equilibrium equation. The Dirichlet boundary condition (2.5) means that the elasticity body is clamped on Γ_D, while (2.6) reflects the surface traction condition on Γ_N. The relations in (2.7) describe the damping response of the foundation. Here, $g > 0$ represents the thickness of a soft layer covering Γ_C, and $g \in L^\infty(\Gamma_C)$. $p \ge 0$ denotes a normal compliance function that characterizes the reaction of the soft layer based on the current penetration value. Coulomb's law of dry friction is modeled by (2.8). Here, μ represents the friction coefficient, $\boldsymbol{n}^*$ is defined in (2.2), where we assume that the magnitude of $\boldsymbol{v}^*$ is significantly greater than that of the tangential velocity $\boldsymbol{u}'_\tau$, making $\boldsymbol{u}'_\tau$ negligible, so we approximate the relative slip rate by $\boldsymbol{v}^*$. Evolution of the wear function is described by (2.9)–(2.10), α is given by (2.2). A detailed derivation of this model can be found in [29].

The contact problem will be studied through its weak formulation. To introduce the weak formulation, we first recall that the inner products on the Hilbert spaces $L^2(\Omega)^d$ and $L^2(\Gamma)^d$ are given by

$$(\boldsymbol{u}, \boldsymbol{v})_{L^2(\Omega)^d} = \int_\Omega \boldsymbol{u} \cdot \boldsymbol{v}\, dx, \quad (\boldsymbol{u}, \boldsymbol{v})_{L^2(\Gamma)^d} = \int_\Gamma \boldsymbol{u} \cdot \boldsymbol{v}\, ds.$$

For a normed space X, let $C([0,T];X])$ be the space of continuous functions from $[0,T]$ to X. We introduce the following Hilbert spaces:

$$Q = L^2(\Omega; \mathbb{S}^d), \quad V = \{\boldsymbol{v} \in H^1(\Omega)^d : \boldsymbol{v} = \boldsymbol{0} \text{ on } \Gamma_D\}$$

endowed with the inner scalar products

$$(\boldsymbol{\sigma}, \boldsymbol{\tau})_Q = \int_\Omega \sigma_{ij}\tau_{ij}\, dx, \quad (\boldsymbol{u}, \boldsymbol{v})_V = (\mathcal{C}\boldsymbol{\varepsilon}(\boldsymbol{u}), \boldsymbol{\varepsilon}(\boldsymbol{v}))_Q$$

with the corresponding norms $\|\cdot\|_Q$ and $\|\cdot\|_V$, where the operator $\mathcal{C}$ satisfies the conditions listed in $H(\mathcal{C})$ below. Since $\text{meas}(\Gamma_D) > 0$, by Korn's inequality ([11]), we know that the space $(V, \|\cdot\|_V)$ is complete and

$$\|\boldsymbol{v}\|_{(H^1(\Omega))^d} \le c\|\boldsymbol{v}\|_V. \tag{2.11}$$

Here and after, we denote by $c > 0$ a generic constant, whose value may differ in different places. Further, in combination with the Sobolev trace theorem, there exists a constant $c_0 > 0$ depending only on Ω, Γ_D and Γ_C, such that

$$\|\boldsymbol{v}\|_{L^2(\Gamma_C)^d} \le c_0\|\boldsymbol{v}\|_V \quad \forall \boldsymbol{v} \in V. \tag{2.12}$$

Denote by $\langle\cdot,\cdot\rangle_{V\times V^*}$ the dual pairing between V and V^*. The set of permissible displacements is

$$U = \{\boldsymbol{v} \in V : v_\nu \le g \text{ on } \Gamma_C\}.$$

The space for the wear function w is

$$W = L^2(\Gamma_C).$$

Next, we introduce the hypotheses on the data needed in the study of Problem 2.1.

$H(\mathcal{C})$: $\mathcal{C} : \Omega \times \mathbb{S}^d \to \mathbb{S}^d$ is such that

$$\begin{array}{l} (a)\ \mathcal{C}(\cdot, \boldsymbol{\varepsilon}) \text{ is measurable on } \Gamma_C\ \forall \boldsymbol{\varepsilon} \in \mathbb{S}^d,\ \mathcal{C}(\cdot, \boldsymbol{0}) \in Q; \\ (b) \text{ for a constant } L_\mathcal{C} > 0,\ \|\mathcal{C}(\boldsymbol{x}, \boldsymbol{\varepsilon}_1) - \mathcal{C}(\boldsymbol{x}, \boldsymbol{\varepsilon}_2)\| \le L_\mathcal{C}\|\boldsymbol{\varepsilon}_1 - \boldsymbol{\varepsilon}_2\|, \\ \quad \forall \boldsymbol{\varepsilon}_1, \boldsymbol{\varepsilon}_2 \in \mathbb{S}^d, \text{ a.e. } \boldsymbol{x} \in \Omega; \\ (c) \text{ for a constant } m_\mathcal{C} > 0,\ (\mathcal{C}(\boldsymbol{x}, \boldsymbol{\varepsilon}_1) - \mathcal{C}(\boldsymbol{x}, \boldsymbol{\varepsilon}_2)) \cdot (\boldsymbol{\varepsilon}_1 - \boldsymbol{\varepsilon}_2) \ge m_\mathcal{C}\|\boldsymbol{\varepsilon}_1 - \boldsymbol{\varepsilon}_2\|^2, \\ \quad \forall \boldsymbol{\varepsilon}_1, \boldsymbol{\varepsilon}_2 \in \mathbb{S}^d, \text{ a.e. } \boldsymbol{x} \in \Omega. \end{array} \tag{2.13}$$

$H(p)$: $p : \Gamma_C \times \mathbb{R} \to \mathbb{R}_+$ is such that

$$
\begin{aligned}
&(a)\ p(\cdot,r) \text{ is measurable on } \Gamma_C\ \forall\, r\in\mathbb{R};\\
&(b)\ \exists\, L_p>0, \text{ s.t. } |p(\boldsymbol{x},r_1)-p(\boldsymbol{x},r_2)|\le L_p|r_1-r_2|\ \forall\, r_1,r_2\in\mathbb{R},\ \text{a.e. } \boldsymbol{x}\in\Gamma_C;\\
&(c)\ (p(\boldsymbol{x},r_1)-p(\boldsymbol{x},r_2))(r_1-r_2)\ge 0\ \forall\, r_1,r_2\in\mathbb{R},\ \text{a.e. } \boldsymbol{x}\in\Gamma_C;\\
&(d)\ p(\boldsymbol{x},r)=0\ \forall\, r\le 0,\ \text{a.e. } \boldsymbol{x}\in\Gamma_C.
\end{aligned}
\tag{2.14}
$$

$H(f)$:

$$
\boldsymbol{f}_1\in C([0,T];L^2(\Omega)^d),\quad \boldsymbol{f}_2\in C([0,T];L^2(\Gamma_N)^d). \tag{2.15}
$$

H_0:

$$
\begin{aligned}
&(a)\ \mu\in L^\infty(\Gamma_C),\ \mu(\boldsymbol{x})\ge 0 \text{ a.e. } \boldsymbol{x}\in\Gamma_C;\\
&(b)\ \kappa\in L^\infty(\Gamma_C),\ \kappa(\boldsymbol{x})\ge 0 \text{ a.e. } \boldsymbol{x}\in\Gamma_C;\\
&(c)\ \boldsymbol{v}^*\in C([0,T];\mathbb{R}^d),\ \|\boldsymbol{v}^*(t)\|\ge v_0>0\ \forall\, t\in[0,T].
\end{aligned}
\tag{2.16}
$$

H_s:

$$
c_0^2 L_p\|\mu\|_{L^\infty(\Gamma_C)}<m_C. \tag{2.17}
$$

From the hypotheses H_0, we know that

$$
\boldsymbol{n}^*\in C([0,T];\mathbb{R}^d),\quad \alpha\in C([0,T];L^\infty(\Gamma_C)), \tag{2.18}
$$

where $\boldsymbol{n}^*$ and α are defined in (2.2). In the literature (e.g., [23]), a condition such as (2.17) is commonly referred to as a smallness condition. For the contact problem under consideration in this paper, we have the following bound on the magnitude of the friction force on the contact surface Γ_C:

$$
|\boldsymbol{\sigma}_\tau(t)|\le L_p\|\mu\|_{L^\infty(\Gamma_C)}|u_\nu(t)-w(t)|.
$$

Therefore, the condition (2.17) sets an upper bound on the linear growth rate $L_p\|\mu\|_{L^\infty(\Gamma_C)}$ of the magnitude of the friction force with respect to the penetration, as compared to the ellipticity constant m_C of the elasticity operator.

Now we define

$$
a(\boldsymbol{u},\boldsymbol{v})=(C(\boldsymbol{\varepsilon}(\boldsymbol{u})),\boldsymbol{\varepsilon}(\boldsymbol{v}))_Q\quad \forall\,\boldsymbol{u},\boldsymbol{v}\in V, \tag{2.19}
$$

$$
\langle \boldsymbol{f}(t),\boldsymbol{v}\rangle_{V^*\times V}=\int_\Omega \boldsymbol{f}_1(t)\cdot\boldsymbol{v}\,dx+\int_{\Gamma_N}\boldsymbol{f}_2(t)\cdot\boldsymbol{v}\,ds\quad \forall\,\boldsymbol{v}\in V,\ t\in[0,T], \tag{2.20}
$$

$$
\varphi(t,w,\boldsymbol{u},\boldsymbol{v})=\int_{\Gamma_C} p(u_\nu-w)\left(v_\nu+\mu\boldsymbol{n}^*(t)\cdot\boldsymbol{v}_\tau\right)ds\quad \forall\,\boldsymbol{u},\boldsymbol{v}\in V,\ w\in L^2(\Gamma_C),\ t\in[0,T]. \tag{2.21}
$$

The next result is shown in [24, Theorem 4, (27)].

Lemma 2.2. *Assume $H(p)$ and H_0. Then for any $t\in[0,T]$, any $\boldsymbol{u}_1,\boldsymbol{u}_2,\boldsymbol{v}_1,\boldsymbol{v}_2\in V$ and any $w_1,w_2\in W$,*

$$
\begin{aligned}
&\varphi(t,w_1,\boldsymbol{u}_1,\boldsymbol{v}_2)+\varphi(t,w_2,\boldsymbol{u}_2,\boldsymbol{v}_1)-\varphi(t,w_1,\boldsymbol{u}_1,\boldsymbol{v}_1)-\varphi(t,w_2,\boldsymbol{u}_2,\boldsymbol{v}_2)\\
&\quad\le L_p\left(\|\boldsymbol{u}_1-\boldsymbol{u}_2\|_{L^2(\Gamma_C)^d}+\|w_1-w_2\|_W\right)\left(\|\mu\|_{L^\infty(\Gamma_C)}\|\boldsymbol{v}_1-\boldsymbol{v}_2\|_{L^2(\Gamma_C)^d}+\|w_1-w_2\|_W\right).
\end{aligned}
$$

Moreover, by the trace inequality (2.12),

$$
\begin{aligned}
&\varphi(t,w_1,\boldsymbol{u}_1,\boldsymbol{v}_2)+\varphi(t,w_2,\boldsymbol{u}_2,\boldsymbol{v}_1)-\varphi(t,w_1,\boldsymbol{u}_1,\boldsymbol{v}_1)-\varphi(t,w_2,\boldsymbol{u}_2,\boldsymbol{v}_2)\\
&\quad\le L_p\left(c_0\|\boldsymbol{u}_1-\boldsymbol{u}_2\|_V+\|w_1-w_2\|_W\right)\left(c_0\|\mu\|_{L^\infty(\Gamma_C)}\|\boldsymbol{v}_1-\boldsymbol{v}_2\|_V+\|w_1-w_2\|_W\right).
\end{aligned}
\tag{2.22}
$$

The weak formulation of Problem 2.1 is the following ([29, Problem $\mathcal{P}^V$]).

Problem 2.3. *Find $\boldsymbol{u}:[0,T]\to U$ and $w:[0,T]\to W$ such that for $t\in[0,T]$,*

$$
\begin{aligned}
&a(\boldsymbol{u}(t),\boldsymbol{v}-\boldsymbol{u}(t))+\varphi(t,w(t),\boldsymbol{u}(t),\boldsymbol{v})-\varphi(t,w(t),\boldsymbol{u}(t),\boldsymbol{u}(t))\\
&\qquad\qquad\ge\langle \boldsymbol{f}(t),\boldsymbol{v}-\boldsymbol{u}(t)\rangle_{V^*\times V}\quad\forall\,\boldsymbol{v}\in U,
\end{aligned}
\tag{2.23}
$$

$$
w(t)=\int_0^t \alpha(s)\,p(u_\nu(s)-w(s))\,ds. \tag{2.24}
$$

Let us recall an existence and uniqueness result for Problem 2.3 from [29, Theorem 4.1].

Theorem 2.4. *Assume $H(C)$, $H(p)$, $H(f)$, H_0 and H_s. Then Problem 2.3 has a unique solution $(\boldsymbol{\sigma}, \boldsymbol{u}, w)$ with*

$$\boldsymbol{\sigma} \in C([0,T]; Q), \quad \boldsymbol{u} \in C([0,T]; V), \quad w \in C^1([0,T]; W).$$

Moreover, $w(t) \geq 0$ for all $t \in [0,T]$, a.e. on Γ_C.

Since $w(t) \geq 0$ a.e. on Γ_C for all $t \in [0,T]$, due to $H(p)(d)$, we have

$$\varphi(t, w(t), \mathbf{0}, \boldsymbol{v}) = 0 \quad \forall \boldsymbol{v} \in V. \tag{2.25}$$

3. A fully discrete scheme

In this section, we introduce a fully discrete scheme to solve Problem 2.3. We apply the virtual element method to discretize the variational inequality (2.23). For simplicity, we only consider the case where Ω is a two-dimensional polygonal domain.

We start by considering a family of decompositions $\{\mathcal{T}_h\}_h$ of $\overline{\Omega}$ into polygonal elements. Denote $h_K = \mathrm{diam}(K)$ for a generic element $K \in \mathcal{T}$ and $h = \max\{h_K : K \in \mathcal{T}_h\}$. All the subdivisions are compatible with the boundary splitting in the sense that if an edge of an element has a non-trivial intersection with one of the three boundary subsets, $\overline{\Gamma_D}$ or $\overline{\Gamma_N}$ or $\overline{\Gamma_C}$, then the edge lies entirely on that subset. Furthermore, we assume that Γ_C is split as $\overline{\Gamma_C} = \cup_{1\leq i\leq I}\Gamma_{C,i}$, each $\Gamma_{C,i}$ being a closed line segment. Let $\mathcal{E}_h^0$ denote the set of all the edges of $\mathcal{T}_h$ excluding the edges on $\overline{\Gamma_D}$, and let $\mathcal{P}_h^0$ denote the set of all the vertices of $\mathcal{T}_h$ excluding the vertices at $\overline{\Gamma_D}$. Following [5], we make the following assumption on the decompositions $\{\mathcal{T}_h\}_h$:

A1. There exist positive constants γ_1 and γ_2 such that for each h and for every $K \in \mathcal{T}_h$,
- K is star-shaped with respect to a disk of radius $\rho \geq \gamma_1 h_K$;
- the distance between any two vertices of K is no less than $\gamma_2 h_K$.

3.1. Construction of V_h

Given a decomposition $\mathcal{T}_h$, we construct a finite-dimensional subspace V_h of V. Similar to the virtual element method employed for the elasticity problem in [4,31], we define, for every element $K \in \mathcal{T}_h$ and integer $k \geq 1$, the local space

$$V_h^K := \{\boldsymbol{v} \in [H^1(K)]^2 : \mathrm{div}\boldsymbol{\sigma}(\boldsymbol{v}) \in [\mathbb{P}_{k-2}(K)]^2, \boldsymbol{v}|_{\partial K} \in C^0(\partial K), \boldsymbol{v}|_e \in [\mathbb{P}_k(e)]^2\ \forall e \subset \partial K\},$$

where $\mathbb{P}_k(K)$ represents the space of polynomials on K of degree no more than k. By convention, $\mathbb{P}_{-1}(K) = \{0\}$. Any $\boldsymbol{v}_h \in V_h^K$ can be determined by the following degrees of freedom:

- values of $\boldsymbol{v}_h$ at the vertices of K;
- moments $\int_e \boldsymbol{q} \cdot \boldsymbol{v}_h\, ds$ for $\boldsymbol{q} \in [\mathbb{P}_{k-2}(e)]^2$ on each edge $e \subset \partial K$ for $k \geq 2$;
- moments $\int_K \boldsymbol{q} \cdot \boldsymbol{v}_h\, dx$ for $\boldsymbol{q} \in [\mathbb{P}_{k-2}(K)]^2$ for $k \geq 2$.

Then, the global virtual element space is

$$V_h := \{\boldsymbol{v} \in V : \boldsymbol{v}|_K \in V_h^K\ \forall K \in \mathcal{T}_h\}, \tag{3.1}$$

and the corresponding global degrees of freedom for $\boldsymbol{v}_h \in V_h$ are

- values of $\boldsymbol{v}_h(\boldsymbol{a}) \quad \forall$ vertex $\boldsymbol{a} \in \mathcal{P}_h^0$;
- moments $\int_e \boldsymbol{q} \cdot \boldsymbol{v}_h\, ds$ for $\boldsymbol{q} \in [\mathbb{P}_{k-2}(e)]^2 \quad \forall e \in \mathcal{E}_h^0$ for $k \geq 2$;
- moments $\int_K \boldsymbol{q} \cdot \boldsymbol{v}_h\, dx$ for $\boldsymbol{q} \in [\mathbb{P}_{k-2}(K)]^2 \quad \forall K \in \mathcal{T}_h$ for $k \geq 2$.

For $k = 1, 2$, the local degrees of freedom for V_h^K are shown in Fig. 1. For the virtual element space, we have the inclusion $[\mathbb{P}_k(K)]^2 \subset V_h^K$, which guarantees the precision of approximation. According to the Scott-Dupont theory ([7,11]), we can derive the following approximation results.

Proposition 3.1. *Let Assumption **A1** be satisfied. For any $\boldsymbol{v} \in [H^l(\Omega)]^2$, $2 \leq l \leq k+1$, there exist $\boldsymbol{v}_I \in V_h$ and $\boldsymbol{v}_\pi \in [\mathbb{P}_k(K)]^2$ such that*

$$\|\boldsymbol{v} - \boldsymbol{v}_I\|_V \leq c\, h^{l-1} |\boldsymbol{v}|_{[H^l(\Omega)]^2}, \tag{3.2}$$

$$\|\boldsymbol{v} - \boldsymbol{v}_\pi\|_{V,K} \leq c\, h_K^{l-1} |\boldsymbol{v}|_{[H^l(K)]^2}, \tag{3.3}$$

where $\|\boldsymbol{v}\|_{V,K}^2 := \int_K \boldsymbol{\varepsilon}(\boldsymbol{v}) : \boldsymbol{\varepsilon}(\boldsymbol{v})\, dx$.

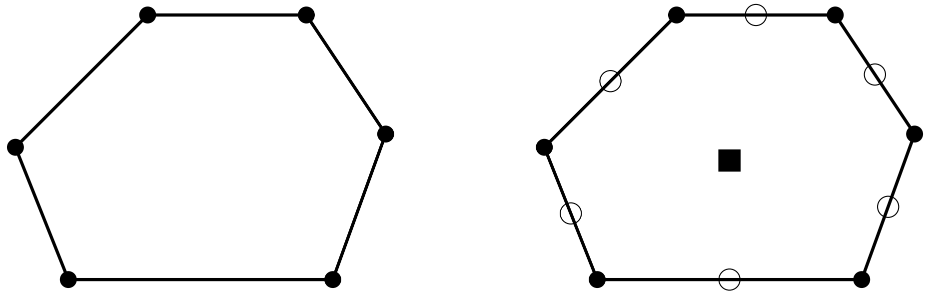

Fig. 1. Local degrees of freedom of V_h^K for $k=1$ (left) and $k=2$ (right).

In the analysis of the virtual element method, we employ a broken norm $\|\cdot\|_{V,h}$ defined by

$$\|\boldsymbol{v}\|_{V,h}^2 = \sum_{K\in\mathcal{T}_h} \|\boldsymbol{v}\|_{V,K}^2.$$

Then we establish the discrete admissible set of virtual elements

$$U_h = \{\boldsymbol{v}_h \in V_h : v_\nu^h \le g \text{ at all nodes on } \Gamma_C\}. \tag{3.4}$$

We assume that g is a concave function, thereby implying that U_h is a subset of U.

Remark 3.2. It is possible to extend the analysis of the numerical method without assuming g to be concave, cf. e.g., [15]. To avoid the additional technicality, in this paper we only consider the case where g is concave.

3.2. Construction of a_h

The bilinear form $a(\cdot,\cdot)$ can be decomposed into its constituent parts by

$$a(\boldsymbol{u},\boldsymbol{v}) = \sum_{K\in\mathcal{T}_h} a^K(\boldsymbol{u},\boldsymbol{v}) \quad \forall\, \boldsymbol{u},\boldsymbol{v}\in V, \tag{3.5}$$

where

$$a^K(\boldsymbol{u},\boldsymbol{v}) = \int_K C\boldsymbol{\varepsilon}(\boldsymbol{u}) : \boldsymbol{\varepsilon}(\boldsymbol{v})\, dx.$$

Accordingly, we formulate appropriate local bilinear forms $a_h^K(\boldsymbol{u},\boldsymbol{v})$ and combine them collectively

$$a_h(\boldsymbol{u}_h,\boldsymbol{v}_h) = \sum_{K\in\mathcal{T}_h} a_h^K(\boldsymbol{u}_h,\boldsymbol{v}_h).$$

According to the general framework of the virtual element method ([3]), the local bilinear form $a_h^K(\boldsymbol{u},\boldsymbol{v})$ should adhere to the following two properties:

• Polynomial consistency:

$$a_h^K(\boldsymbol{v}_h,\boldsymbol{q}) = a^K(\boldsymbol{v}_h,\boldsymbol{q}) \quad \forall\, \boldsymbol{v}_h \in V_h^K,\ \forall\, \boldsymbol{q}\in[\mathbb{P}_k(K)]^2. \tag{3.6}$$

• Stability: there exist two positive constants α_* and α^*, independent of h and K, s.t.

$$\alpha_* a^K(\boldsymbol{v}_h,\boldsymbol{v}_h) \le a_h^K(\boldsymbol{v}_h,\boldsymbol{v}_h) \le \alpha^* a^K(\boldsymbol{v}_h,\boldsymbol{v}_h) \quad \forall\, \boldsymbol{v}_h \in V_h^K. \tag{3.7}$$

Since the basis functions are unavailable for V_h^K, direct computation of the value of $a^K(\boldsymbol{u},\boldsymbol{v})$ for $\boldsymbol{u},\boldsymbol{v}\in V_h$ is not feasible. In order to ensure the computability, we have devised a projection operator $\Pi_k^K : V_h^K \to [\mathbb{P}_k(K)]^2$ by

$$a^K(\Pi_k^K \boldsymbol{v}_h - \boldsymbol{v}_h, \boldsymbol{q}) = 0 \quad \forall\, \boldsymbol{q}\in[\mathbb{P}_k(K)]^2, \tag{3.8}$$

$$\frac{1}{n_V^K}\sum_{i=1}^{n_V^K} \Pi_k^K \boldsymbol{v}_h(\boldsymbol{x}_i) = \frac{1}{n_V^K}\sum_{i=1}^{n_V^K} \boldsymbol{v}_h(\boldsymbol{x}_i), \tag{3.9}$$

$$\frac{1}{n_V^K}\sum_{i=1}^{n_V^K} \boldsymbol{x}_i \times \Pi_k^K \boldsymbol{v}_h(\boldsymbol{x}_i) = \frac{1}{n_V^K}\sum_{i=1}^{n_V^K} \boldsymbol{x}_i \times \boldsymbol{v}_h(\boldsymbol{x}_i), \tag{3.10}$$

where $\{\boldsymbol{x}_i\}$ are the coordinates of the vertices of the element K and n_V^K denotes the number of the vertices ([37]). Note that (3.8) alone determines $\Pi_k^K \boldsymbol{v}_h$ only up to a rigid motion, and we add the conditions (3.9)–(3.10) by adopting an idea in [31].

Then, we proceed to define the local bilinear form

$$a_h^K(\boldsymbol{u}_h, \boldsymbol{v}_h) = a^K(\Pi_k^K \boldsymbol{u}_h, \Pi_k^K \boldsymbol{v}_h) + S^K(\boldsymbol{u}_h - \Pi_k^K \boldsymbol{u}_h, \boldsymbol{v}_h - \Pi_k^K \boldsymbol{v}_h) \quad \forall \boldsymbol{u}_h, \boldsymbol{v}_h \in V_h^K, \tag{3.11}$$

where the stabilization term $S^K(\boldsymbol{u}_h, \boldsymbol{v}_h)$ is chosen to satisfy

$$c_4 a^K(\boldsymbol{v}_h, \boldsymbol{v}_h) \le S^K(\boldsymbol{v}_h, \boldsymbol{v}_h) \le c_5 a^K(\boldsymbol{v}_h, \boldsymbol{v}_h) \quad \forall \boldsymbol{v}_h \in V_h^K \text{ with } \Pi_k^K \boldsymbol{v}_h = \boldsymbol{0} \tag{3.12}$$

with two positive constants c_4 and c_5. It is not difficult to verify that (3.8)–(3.12) ensures the properties (3.6) and (3.7). In this paper, we have opted for

$$S^K(\boldsymbol{u}_h, \boldsymbol{v}_h) = \sum_{i=1}^{N_K^{\text{dof}}} \chi_i(\boldsymbol{u}_h)\, \chi_i(\boldsymbol{v}_h),$$

where $\chi_i(\boldsymbol{u}_h)$ denotes the i-th degree of freedom for $\boldsymbol{u}_h$ and N_K^{dof} is the number of local degrees of freedom.

Define

$$a_h(\boldsymbol{u}_h, \boldsymbol{v}_h) = \sum_{K \in \mathcal{T}_h} a_h^K(\boldsymbol{u}_h, \boldsymbol{v}_h) \quad \forall \boldsymbol{u}_h, \boldsymbol{v}_h \in V_h.$$

As a consequence of the symmetry of a_h, stability (3.7) and (3.12), there exist two positive constants C_1 and C_2 such that

$$a_h(\boldsymbol{v}_h, \boldsymbol{v}_h) \ge C_1 \|\boldsymbol{v}_h\|_V^2 \quad \forall \boldsymbol{v}_h \in V_h, \tag{3.13}$$

$$a_h(\boldsymbol{u}_h, \boldsymbol{v}_h) \le C_2 \|\boldsymbol{u}_h\|_V \|\boldsymbol{v}_h\|_V \quad \forall \boldsymbol{u}_h, \boldsymbol{v}_h \in V_h. \tag{3.14}$$

3.3. Construction of $\boldsymbol{f}_h$

Since the term $\int_\Omega \boldsymbol{f}_1 \cdot \boldsymbol{v}\, dx$ is not computable for $\boldsymbol{v} \in V_h$, we introduce its approximation. Let P_k^K be the $L^2(K)$ projection from V_h^K to $[\mathbb{P}_k(K)]^2$. The node average of the function ϕ on the cell K is defined as follows:

$$\hat{\phi} := \frac{1}{n_K} \sum_{i=1}^{n_K} \phi(v_i), \tag{3.15}$$

where n_K is the number of vertices of the element K, and v_i, $1 \le i \le n_K$, are the vertices of K.

For $k = 1$, we define

$$\langle \boldsymbol{f}_{1h}, \boldsymbol{v}_h \rangle = \sum_{K \in \mathcal{T}_h} \int_K P_0^K \boldsymbol{f}_1 \cdot \widehat{\boldsymbol{v}_h}\, dx \quad \forall \boldsymbol{v}_h \in V_h.$$

For $k \ge 2$, we define

$$\langle \boldsymbol{f}_{1h}, \boldsymbol{v}_h \rangle = \sum_{K \in \mathcal{T}_h} \int_K P_{k-2}^K \boldsymbol{f}_1 \cdot \boldsymbol{v}_h\, dx \quad \forall \boldsymbol{v}_h \in V_h.$$

To approximate the right-hand side term $\langle \boldsymbol{f}_h, \boldsymbol{v}_h \rangle_{V^* \times V}$, we choose

$$\langle \boldsymbol{f}_h, \boldsymbol{v}_h \rangle = \langle \boldsymbol{f}_{1h}, \boldsymbol{v}_h \rangle + \int_{\Gamma_N} \boldsymbol{f}_2 \cdot \boldsymbol{v}_h\, ds \quad \forall \boldsymbol{v}_h \in V_h.$$

It is not difficult to verify that $\langle \boldsymbol{f}_h, \boldsymbol{v}_h \rangle$ can be computed with the given degrees of freedom. We have the following approximation property ([4])

$$\|\boldsymbol{f}_1 - \boldsymbol{f}_{1h}\|_{V_h'} = \sup_{\boldsymbol{v}_h \in V_h} \frac{(\boldsymbol{f}_1, \boldsymbol{v}_h) - \langle \boldsymbol{f}_{1h}, \boldsymbol{v}_h \rangle}{\|\boldsymbol{v}_h\|_V} \le c\, h^k |\boldsymbol{f}_1|_{k-1}. \tag{3.16}$$

Also,

$$\langle \boldsymbol{f}, \boldsymbol{v}_h \rangle_{V^* \times V} - \langle \boldsymbol{f}_h, \boldsymbol{v}_h \rangle \le \|\boldsymbol{f}_1 - \boldsymbol{f}_{1h}\|_{V_h'} \|\boldsymbol{v}_h\|_V \quad \forall \boldsymbol{v}_h \in V_h. \tag{3.17}$$

Furthermore, by the property of the L^2 projection operator P_k^K, we have

$$\langle \boldsymbol{f}_h, \boldsymbol{v}_h \rangle \le c\, \|\boldsymbol{v}_h\|_V \quad \forall \boldsymbol{v}_h \in V_h, \tag{3.18}$$

where the constant c depends on $\boldsymbol{f}_1$, $\boldsymbol{f}_2$, and the measurement of the domain Ω.

3.4. The fully discrete scheme

Problem 2.3 is time-dependent. We use the VEM to discretize the variational inequality (2.23) for the spatial variable, and use the left rectangle numerical integration formula to approximate the integral equation (2.24).

Let $W_h \subset W$ be a finite-dimensional space. Consider a partition of the time interval $[0,T]$ given by $0 = t_0 < t_1 < \cdots < t_N = T$. Denote $k_n = t_{n+1} - t_n$, $0 \le n \le N-1$, and $k = \max_{0\le n\le N-1} k_n$ for the time step-size. For a function z continuous in t, we use the notation $z^n = z(t_n)$. In addition, we make the following smoothness assumption:
H_a: The solution $\boldsymbol{u}$ of Problem 2.3 and the velocity of the foundation $\boldsymbol{v}^*$ satisfy

$$\boldsymbol{u} \in H^1(0,T;V), \quad \boldsymbol{v}^* \in W^{1,\infty}(0,T;\mathbb{R}^2). \tag{3.19}$$

Note that assumptions $H_0(b)$ and H_a imply that

$$\alpha \in W^{1,\infty}\left(0,T;L^\infty(\Gamma_C)\right). \tag{3.20}$$

Consider the following fully discrete scheme for Problem 2.3.

Problem 3.3. *Find $\boldsymbol{u}_h^n \in U_h$, $0 \le n \le N$ and $w_h^n \in W_h$, $1 \le n \le N$, such that*

$$a_h(\boldsymbol{u}_h^n, \boldsymbol{v}_h - \boldsymbol{u}_h^n) + \varphi(t_n, w_h^n, \boldsymbol{u}_h^n, \boldsymbol{v}_h) - \varphi(t_n, w_h^n, \boldsymbol{u}_h^n, \boldsymbol{u}_h^n) \ge \langle \boldsymbol{f}_h, \boldsymbol{v}_h - \boldsymbol{u}_h^n\rangle \quad \forall \boldsymbol{v}_h \in U_h, \tag{3.21}$$

$$w_h^n = \sum_{j=0}^{n-1} k_j \alpha^j p(u_{h,\nu}^j - w_h^j), \tag{3.22}$$

$$w_h^0 = 0. \tag{3.23}$$

Theorem 3.4. *Keep the assumptions stated in Theorem 2.4. Moreover, assume a smallness condition $C_1 > c_0^2 L_p \|\mu\|_{L^\infty(\Gamma_C)}$, where C_1 is the constant in the inequality (3.13), c_0 is the constant in the trace inequality (2.12), L_p is the Lipschitz constant of the normal compliance function p, μ is the friction coefficient. Then Problem 3.3 has a unique solution.*

Proof. The result is proved by an induction. Note that w_h^0 is given by (3.23). For $0 \le n \le N$, with w_h^n defined by (3.22), let us prove that (3.21) uniquely determines an element $\boldsymbol{u}_h^n \in U_h$. For this purpose, we apply a standard result, see, e.g., [28, Theorem 2.19].

Consider the operator $A_h : V_h \to V_h'$ defined by

$$\langle A_h \boldsymbol{u}_h, \boldsymbol{v}_h\rangle := a_h(\boldsymbol{u}_h, \boldsymbol{v}_h) \quad \forall \boldsymbol{u}_h, \boldsymbol{v}_h \in V_h. \tag{3.24}$$

By the continuity of a_h in (3.14), we see that A_h is Lipschitz continuous on V_h,

$$\|A_h \boldsymbol{u}_h - A_h \boldsymbol{v}_h\|_V \le C_2 \|\boldsymbol{u}_h - \boldsymbol{v}_h\|_V \quad \forall \boldsymbol{u}_h,\, \boldsymbol{v}_h \in V_h. \tag{3.25}$$

In addition, by the coerciveness of a_h in (3.13), we have

$$(A_h \boldsymbol{u}_h - A_h \boldsymbol{v}_h, \boldsymbol{u}_h - \boldsymbol{v}_h) = a_h(\boldsymbol{u}_h - \boldsymbol{v}_h, \boldsymbol{u}_h - \boldsymbol{v}_h) \ge C_1 \|\boldsymbol{u}_h - \boldsymbol{v}_h\|_V^2 \quad \forall \boldsymbol{u}_h, \boldsymbol{v}_h \in V_h. \tag{3.26}$$

By (3.25)–(3.26), A_h is a strongly monotone Lipschitz continuous operator on V_h.

Second, note that for all $\boldsymbol{u}_h \in V_h$, the functional $\varphi(t_n, w_h^n, \boldsymbol{u}_h, \cdot)$ is convex. Let us show that $\varphi(t_n, w_h^n, \boldsymbol{u}_h, \cdot)$ is Lipschitz continuous. Based on the definition, it is required that $w_h^n \ge 0$ and $u_{h,\nu}^n \le g$. By the assumption $H(p)(b)$, $H(p)(d)$, assumption H_0 and trace inequality (2.12), given $\boldsymbol{u}_h$, for all $\boldsymbol{v}_{h1}, \boldsymbol{v}_{h2} \in V_h$,

$$\begin{aligned}
&|\varphi(t_n, w_h^n, \boldsymbol{u}_h, \boldsymbol{v}_{h1}) - \varphi(t_n, w_h^n, \boldsymbol{u}_h, \boldsymbol{v}_{h2})| \\
&\quad = |\int_{\Gamma_C} \left(p(u_{h,\nu}^n - w_h^n) - 0\right)\left((v_{h1,\nu} - v_{h2,\nu}) + \mu \boldsymbol{n}^*(t)\cdot(\boldsymbol{v}_{h1,\tau} - \boldsymbol{v}_{h2,\tau})\right) ds| \\
&\quad \le L_p \int_{\Gamma_C} |u_{h,\nu}^n - w_h^n|\, |(v_{h1,\nu} - v_{h2,\nu}) + \mu \boldsymbol{n}^*(t)\cdot(\boldsymbol{v}_{h1,\tau} - \boldsymbol{v}_{h2,\tau})| ds \\
&\quad \le L_p \|g\|_{L^\infty(\Gamma_C)} \int_{\Gamma_C} |(v_{h1,\nu} - v_{h2,\nu}) + \mu \boldsymbol{n}^*(t)\cdot(\boldsymbol{v}_{h1,\tau} - \boldsymbol{v}_{h2,\tau})| ds \\
&\quad \le c_0 \|g\|_{L^\infty(\Gamma_C)} L_p (1 + \|\mu\|_{L^\infty(\Gamma_C)}) \|\boldsymbol{v}_{h1} - \boldsymbol{v}_{h2}\|_V.
\end{aligned} \tag{3.27}$$

Therefore, $\varphi(t_n, w_h^n, \boldsymbol{u}_h, \cdot)$ is convex and lower semi-continuous. In addition, by Lemma 2.2, we get

$$\varphi(t_n, w_h^n, \boldsymbol{u}_{h1}, \boldsymbol{v}_{h2}) + \varphi(t_n, w_h^n, \boldsymbol{u}_{h2}, \boldsymbol{v}_{h1}) - \varphi(t_n, w_h^n, \boldsymbol{u}_{h1}, \boldsymbol{v}_{h1}) - \varphi(t_n, w_h^n, \boldsymbol{u}_{h2}, \boldsymbol{v}_{h2})$$
$$\leq c_0^2 L_p \|\mu\|_{L^\infty(\Gamma_C)} \|\boldsymbol{u}_{h1} - \boldsymbol{u}_{h2}\|_V \|\boldsymbol{v}_{h1} - \boldsymbol{v}_{h2}\|_V \quad \forall \boldsymbol{u}_{h1}, \boldsymbol{u}_{h2}, \boldsymbol{v}_{h1}, \boldsymbol{v}_{h2} \in V_h. \tag{3.28}$$

Finally, thanks to the smallness condition $C_1 > c_0^2 L_p \|\mu\|_{L^\infty(\Gamma_C)}$, we apply an argument similar to that in the proof of [28, Theorem 2.19] to deduce that there exists a unique element $\boldsymbol{u}_h^n \in U_h$ such that (3.21) holds. ■

4. Error estimates

In the numerical analysis, we will make use of the following discrete Gronwall inequality ([22, Lemma 7.25]).

Lemma 4.1. *Assume $\{g_n\}_{n=1}^N$ and $\{e_n\}_{n=1}^N$ are two sequences of non-negative numbers satisfying*

$$e_n \leq c g_n + c \sum_{j=1}^{n-1} k_j e_j, \quad n = 1, \cdots, N.$$

Then,

$$e_n \leq c \left(g_n + \sum_{j=1}^{n-1} k_j g_j \right), \quad n = 1, \cdots, N.$$

Therefore,

$$\max_{1 \leq n \leq N} e_n \leq c \max_{1 \leq n \leq N} g_n.$$

First, we provide a uniform boundedness result on the numerical solution $\boldsymbol{u}_h$.

Lemma 4.2. *Under the assumptions stated in Theorem 3.4, for $0 \leq n \leq N$, the numerical solution $\boldsymbol{u}_h^n \in U_h$ is uniformly bounded independent of h.*

Proof. Let $\boldsymbol{v}_h = \boldsymbol{0} \in V_h$ in (3.21),

$$a_h(\boldsymbol{u}_h^n, -\boldsymbol{u}_h^n) + \varphi(t_n, w_h^n, \boldsymbol{u}_h^n, \boldsymbol{0}) - \varphi(t_n, w_h^n, \boldsymbol{u}_h^n, \boldsymbol{u}_h^n) \geq \langle \boldsymbol{f}_h, -\boldsymbol{u}_h^n \rangle.$$

So

$$a_h(\boldsymbol{u}_h^n, \boldsymbol{u}_h^n) \leq \langle \boldsymbol{f}_h, \boldsymbol{u}_h^n \rangle + \varphi(t_n, w_h^n, \boldsymbol{u}_h^n, \boldsymbol{0}) - \varphi(t_n, w_h^n, \boldsymbol{u}_h^n, \boldsymbol{u}_h^n). \tag{4.1}$$

By (2.25) and Lemma 2.2,

$$\varphi(t_n, w_h^n, \boldsymbol{u}_h^n, \boldsymbol{0}) - \varphi(t_n, w_h^n, \boldsymbol{u}_h^n, \boldsymbol{u}_h^n) = \varphi(t_n, w_h^n, \boldsymbol{u}_h^n, \boldsymbol{0}) - \varphi(t_n, w_h^n, \boldsymbol{u}_h^n, \boldsymbol{u}_h^n)$$
$$+ \varphi(t_n, w_h^n, \boldsymbol{0}, \boldsymbol{u}_h^n) - \varphi(t_n, w_h^n, \boldsymbol{0}, \boldsymbol{0})$$
$$\leq c_0^2 L_p \|\mu\|_{L^\infty(\Gamma_C)} \|\boldsymbol{u}_h^n\|_V^2. \tag{4.2}$$

Apply (3.13), (3.18) and (4.2) in (4.1) to obtain

$$(C_1 - c_0^2 L_p \|\mu\|_{L^\infty(\Gamma_C)}) \|\boldsymbol{u}_h^n\|_V^2 \leq c \|\boldsymbol{u}_h^n\|_V.$$

By the smallness condition $C_1 > c_0^2 L_p \|\mu\|_{L^\infty(\Gamma_C)}$,

$$\|\boldsymbol{u}_h^n\|_V \leq \frac{c}{C_1 - c_0^2 L_p \|\mu\|_{L^\infty(\Gamma_C)}},$$

which completes the proof. ■

Denote the numerical solution errors

$$\boldsymbol{e}^n = \boldsymbol{u}^n - \boldsymbol{u}_h^n, \quad \theta^n = w^n - w_h^n, \quad 0 \leq n \leq N, \tag{4.3}$$

where $(\boldsymbol{u}^n, w^n)$ is the solution of Problem 2.3, and $(\boldsymbol{u}_h^n, w_h^n)$ is the solution of Problem 3.3.

By adapting the proof of Theorem 4 in [24] to the case of non-uniform partition of the time interval, we have the following result.

Lemma 4.3. *Under the assumptions stated in Theorem 3.4 and H_a, we have*

$$\|\theta^n\|_W^2 \le ck^2 + c\sum_{m=0}^{n-1} k_m \left(\|e^m\|_V^2 + \|\theta^m\|_W^2\right), \quad 1 \le n \le N. \tag{4.4}$$

To derive an error estimate for the displacement, we add the following solution regularity assumption:

Assumption 4.4. The contact boundary Γ_C can be expressed as the union of some line segments $\overline{\Gamma_C} = \cup_{i=1}^{I}\Gamma_{C,i}$, and $\Gamma_{C,i} \cap \Gamma_{C,j} = \emptyset$ for $1 \le i < j \le I$. Assume

$$\boldsymbol{u} \in C\left([0,T]; H^2(\Omega)^2\right), \quad \boldsymbol{u}|_{\Gamma_{C,i}} \in C\left([0,T]; H^2(\Gamma_{C,i})\right), \quad \boldsymbol{\sigma\nu} \in C\left([0,T]; L^2(\Gamma_C)^2\right). \tag{4.5}$$

Now we give the error estimates for the displacement.

Lemma 4.5. *Under the assumptions stated in Theorem 3.4 and Assumption 4.4, we have*

$$\begin{aligned}\|\boldsymbol{e}^n\|_V^2 \le{}& c\left(\|\boldsymbol{u}^n - \boldsymbol{u}_\pi^n\|_{V,h} + \|\boldsymbol{u}^n - \boldsymbol{u}_I^n\|_V + \|\boldsymbol{f} - \boldsymbol{f}_h\|_{V_h'}\right)^2\\ &+ c\,\|\theta^n\|_W^2 + c\,\|\boldsymbol{u}^n - \boldsymbol{u}_I^n\|_{L^2(\Gamma_C)}, \quad 0 \le n \le N,\end{aligned} \tag{4.6}$$

where $\boldsymbol{u}_I^n$ is the interpolation of $\boldsymbol{u}^n$, and $\boldsymbol{u}_\pi^n$ is a piecewise polynomial approximation of $\boldsymbol{u}^n$.

Proof. For $n \in \{0, 1, \cdots, N\}$, we split $\boldsymbol{e}^n$ into two parts:

$$\boldsymbol{e}^n = (\boldsymbol{u}^n - \boldsymbol{u}_I^n) + (\boldsymbol{u}_I^n - \boldsymbol{u}_h^n) := \boldsymbol{e}_I^n + \boldsymbol{e}_h^n, \tag{4.7}$$

where $\boldsymbol{u}_I^n \in V_h$ is the interpolation of $\boldsymbol{u}^n$.

By the coerciveness of a_h, setting $\boldsymbol{v}_h = \boldsymbol{e}_h^n = \boldsymbol{u}_I^n - \boldsymbol{u}_h^n \in V_h$ in (3.13), we get

$$C_1\|\boldsymbol{e}_h^n\|_V^2 \le a_h(\boldsymbol{e}_h^n, \boldsymbol{e}_h^n) = a_h(\boldsymbol{u}_I^n, \boldsymbol{e}_h^n) - a_h(\boldsymbol{u}_h^n, \boldsymbol{e}_h^n). \tag{4.8}$$

By the polynomial consistency of a_h in (3.6), we have

$$\begin{aligned}a_h(\boldsymbol{u}_I^n, \boldsymbol{e}_h^n) &= \sum_{K\in\mathcal{T}_h} (a_h^K(\boldsymbol{u}_I^n - \boldsymbol{u}_\pi^n, \boldsymbol{e}_h^n) + a_h^K(\boldsymbol{u}_\pi^n, \boldsymbol{e}_h^n))\\ &= \sum_{K\in\mathcal{T}_h} (a_h^K(\boldsymbol{u}_I^n - \boldsymbol{u}_\pi^n, \boldsymbol{e}_h^n) + a^K(\boldsymbol{u}_\pi^n, \boldsymbol{e}_h^n))\\ &= \sum_{K\in\mathcal{T}_h} (a_h^K(\boldsymbol{u}_I^n - \boldsymbol{u}_\pi^n, \boldsymbol{e}_h^n) + a^K(\boldsymbol{u}_\pi^n - \boldsymbol{u}^n, \boldsymbol{e}_h^n)) + a^K(\boldsymbol{u}^n, \boldsymbol{e}_h^n)).\end{aligned} \tag{4.9}$$

Let $\boldsymbol{v}_h = \boldsymbol{u}_I^n \in V_h$ in (3.21) to obtain

$$\begin{aligned}-a_h(\boldsymbol{u}_h^n, \boldsymbol{e}_h^n) &= -a_h(\boldsymbol{u}_h^n, \boldsymbol{u}_I^n - \boldsymbol{u}_h^n)\\ &\le -\langle \boldsymbol{f}_h, \boldsymbol{u}_I^n - \boldsymbol{u}_h^n\rangle + \varphi(t_n, w_h^n, \boldsymbol{u}_h^n, \boldsymbol{u}_I^n) - \varphi(t_n, w_h^n, \boldsymbol{u}_h^n, \boldsymbol{u}_h^n).\end{aligned} \tag{4.10}$$

Combining (4.8)–(4.10), we have

$$C_1\|\boldsymbol{e}_h^n\|_V^2 \le R_1 + R_2 + R_3, \tag{4.11}$$

where

$$\begin{aligned}R_1 &= \sum_{K\in\mathcal{T}_h} (a_h^K(\boldsymbol{u}_I^n - \boldsymbol{u}_\pi^n, \boldsymbol{e}_h^n) + a_h^K(\boldsymbol{u}_\pi^n - \boldsymbol{u}^n, \boldsymbol{e}_h^n)),\\ R_2 &= \left\langle \boldsymbol{f}, \boldsymbol{e}_h^n\right\rangle_{V^*\times V} - \langle \boldsymbol{f}_h, \boldsymbol{e}_h^n\rangle,\\ R_3 &= a(\boldsymbol{u}^n, \boldsymbol{e}_h^n) - \left\langle \boldsymbol{f}, \boldsymbol{e}_h^n\right\rangle_{V^*\times V} + \varphi(t_n, w_h^n, \boldsymbol{u}_h^n, \boldsymbol{u}_I^n) - \varphi(t_n, w_h^n, \boldsymbol{u}_h^n, \boldsymbol{u}_h^n).\end{aligned}$$

Let us bound each term on the right-hand side of (4.11). From the continuity of each a^K and the Cauchy-Schwarz inequality,

$$R_1 \le c\left((\sum_{K\in\mathcal{T}_h} \|\boldsymbol{u}_I^n - \boldsymbol{u}_\pi^n\|_{V,K}^2)^{1/2} + (\sum_{K\in\mathcal{T}_h} \|\boldsymbol{u}^n - \boldsymbol{u}_\pi^n\|_{V,K}^2)^{1/2}\right)\|\boldsymbol{e}_h^n\|_V. \tag{4.12}$$

From (3.17),

$$R_2 \le C\|\boldsymbol{f}_1 - \boldsymbol{f}_{1h}\|_{V_h'}\|\boldsymbol{e}_h^n\|_V. \tag{4.13}$$

By following the arguments presented in [22, Section 8.1], it can be shown that under Assumption 4.4, the solution of Problem 2.3 satisfies, for $t \in [0, T]$,

$$-\operatorname{div}\boldsymbol{\sigma}(t) = \boldsymbol{f}_1(t) \quad \text{a.e. in } \Omega, \tag{4.14}$$

$$\boldsymbol{\sigma}(t)\boldsymbol{\nu} = \boldsymbol{f}_2(t) \quad \text{a.e. in } \Gamma_N, \tag{4.15}$$

where

$$\boldsymbol{\sigma}(t) = \mathcal{C}\boldsymbol{\varepsilon}(\boldsymbol{u}(t)). \tag{4.16}$$

Multiply both sides of the equation (4.14) at $t = t_n$, $n \in \{0, \cdots, N\}$, by $(\boldsymbol{u}_I^n - \boldsymbol{u}_h^n)$ and integrate over Ω. By Green's formula (2.1) and combining the boundary condition (4.15), we deduce that

$$\begin{aligned} a(\boldsymbol{u}^n, \boldsymbol{e}_h^n) - \left\langle \boldsymbol{f}, \boldsymbol{e}_h^n \right\rangle_{V^*\times V} &= \int_{\Gamma_C} \boldsymbol{\sigma}(t_n)\boldsymbol{\nu}\cdot(\boldsymbol{u}_I^n - \boldsymbol{u}_h^n)\,ds \\ &= \int_{\Gamma_C} \sigma_\nu(t_n)(u_{I\nu}^n - u_{h\nu}^n)\,ds + \int_{\Gamma_C} \boldsymbol{\sigma}_\tau(t_n)\cdot(\boldsymbol{u}_{I\tau}^n - \boldsymbol{u}_{h\tau}^n)\,ds \\ &\le -\int_{\Gamma_C} p(u_\nu^n - w^n)(u_{I\nu}^n - u_{h\nu}^n)\,ds \\ &\quad - \int_{\Gamma_C} \mu\, p(u_\nu^n - w^n)\boldsymbol{n}^*\cdot(\boldsymbol{u}_{I\tau}^n - \boldsymbol{u}_{h\tau}^n)\,ds. \end{aligned} \tag{4.17}$$

By the definition of φ in (2.21), we get

$$a(\boldsymbol{u}^n, \boldsymbol{e}_h^n) - \left\langle \boldsymbol{f}, \boldsymbol{e}_h^n \right\rangle_{V^*\times V} \le -\varphi(t_n, w^n, \boldsymbol{u}^n, \boldsymbol{u}_I^n) + \varphi(t_n, w^n, \boldsymbol{u}^n, \boldsymbol{u}_h^n). \tag{4.18}$$

Use (4.18) to find

$$\begin{aligned} R_3 &\le \varphi(t_n, w_h^n, \boldsymbol{u}_h^n, \boldsymbol{u}_I^n) - \varphi(t_n, w_h^n, \boldsymbol{u}_h^n, \boldsymbol{u}_h^n) - \varphi(t_n, w^n, \boldsymbol{u}^n, \boldsymbol{u}_I^n) + \varphi(t_n, w^n, \boldsymbol{u}^n, \boldsymbol{u}_h^n) \\ &= \left(\varphi(t_n, w^n, \boldsymbol{u}^n, \boldsymbol{u}_h^n) - \varphi(t_n, w^n, \boldsymbol{u}^n, \boldsymbol{u}^n) + \varphi(t_n, w_h^n, \boldsymbol{u}_h^n, \boldsymbol{u}^n) - \varphi(t_n, w_h^n, \boldsymbol{u}_h^n, \boldsymbol{u}_h^n)\right) \\ &\quad + \left(\varphi(t_n, w^n, \boldsymbol{u}^n, \boldsymbol{u}^n) - \varphi(t_n, w^n, \boldsymbol{u}^n, \boldsymbol{u}_I^n)\right) + \left(\varphi(t_n, w_h^n, \boldsymbol{u}_h^n, \boldsymbol{u}_I^n) - \varphi(t_n, w_h^n, \boldsymbol{u}_h^n, \boldsymbol{u}^n)\right). \end{aligned} \tag{4.19}$$

By (2.22) in Lemma 2.2, we get

$$\begin{aligned} &\varphi(t_n, w^n, \boldsymbol{u}^n, \boldsymbol{u}_h^n) - \varphi(t_n, w^n, \boldsymbol{u}^n, \boldsymbol{u}^n) + \varphi(t_n, w_h^n, \boldsymbol{u}_h^n, \boldsymbol{u}^n) - \varphi(t_n, w_h^n, \boldsymbol{u}_h^n, \boldsymbol{u}_h^n) \\ &\le L_p\left(c_0\|\boldsymbol{u}^n - \boldsymbol{u}_h^n\|_V + \|w^n - w_h^n\|_W\right)\left(c_0\|\mu\|_{L^\infty(\Gamma_C)}\|\boldsymbol{u}^n - \boldsymbol{u}_h^n\|_V + \|w^n - w_h^n\|_W\right). \end{aligned} \tag{4.20}$$

By (2.25), $\varphi(t, w, \boldsymbol{0}, \boldsymbol{v}) = 0\ \forall\, \boldsymbol{v} \in V$. By Lemma 2.2, we get

$$\begin{aligned} \varphi(t_n, w^n, \boldsymbol{u}^n, \boldsymbol{u}^n) - \varphi(t_n, w^n, \boldsymbol{u}^n, \boldsymbol{u}_I^n) &= \varphi(t_n, w^n, \boldsymbol{u}^n, \boldsymbol{u}^n) - \varphi(t_n, w^n, \boldsymbol{u}^n, \boldsymbol{u}_I^n) \\ &\quad + \varphi(t_n, w^n, \boldsymbol{0}, \boldsymbol{u}^n) - \varphi(t_n, w^n, \boldsymbol{0}, \boldsymbol{u}_I^n) \\ &\le L_p\|\mu\|_{L^\infty(\Gamma_C)}\|\boldsymbol{u}^n\|_{L^2(\Gamma_C)}\|\boldsymbol{u}^n - \boldsymbol{u}_I^n\|_{L^2(\Gamma_C)}. \end{aligned} \tag{4.21}$$

Similarly, we have

$$\varphi(t_n, w_h^n, \boldsymbol{u}_h^n, \boldsymbol{u}_I^n) - \varphi(t_n, w_h^n, \boldsymbol{u}_h^n, \boldsymbol{u}^n) \le L_p\|\mu\|_{L^\infty(\Gamma_C)}\|\boldsymbol{u}_h^n\|_{L^2(\Gamma_C)}\|\boldsymbol{u}^n - \boldsymbol{u}_I^n\|_{L^2(\Gamma_C)}. \tag{4.22}$$

Substitute (4.20)–(4.22) in (4.19) and use the boundedness results in Lemma 4.2 to obtain

$$\begin{aligned} R_3 &\le c_0^2 L_p\|\mu\|_{L^\infty(\Gamma_C)}\|\boldsymbol{u}^n - \boldsymbol{u}_h^n\|_V^2 + c\|\boldsymbol{u}^n - \boldsymbol{u}_h^n\|_V\|w^n - w_h^n\|_W \\ &\quad + c\|w^n - w_h^n\|_W^2 + c\|\boldsymbol{u}^n - \boldsymbol{u}_I^n\|_{L^2(\Gamma_C)}. \end{aligned} \tag{4.23}$$

Using the Young inequality and triangle inequality

$$\|\boldsymbol{u}^n - \boldsymbol{u}_h^n\|_V \le \|\boldsymbol{u}^n - \boldsymbol{u}_I^n\|_V + \|\boldsymbol{u}_I^n - \boldsymbol{u}_h^n\|_V, \tag{4.24}$$

we get

$$
\begin{aligned}
c_0^2 L_p \|\mu\|_{L^\infty(\Gamma_C)} \|\boldsymbol{u}^n - \boldsymbol{u}_h^n\|_V^2 &= c_0^2 L_p \|\mu\|_{L^\infty(\Gamma_C)} \left(\|\boldsymbol{e}_h^n\|_V^2 + 2\|\boldsymbol{e}_h^n\|_V \|\boldsymbol{u}^n - \boldsymbol{u}_I^n\|_V + \|\boldsymbol{u}^n - \boldsymbol{u}_I^n\|_V^2 \right) \\
&= c_0^2 L_p \|\mu\|_{L^\infty(\Gamma_C)} \|\boldsymbol{e}_h^n\|_V^2 + 2 c_0^2 L_p \|\mu\|_{L^\infty(\Gamma_C)} \|\boldsymbol{e}_h^n\|_V \|\boldsymbol{u}^n - \boldsymbol{u}_I^n\|_V \\
&\quad + c_0^2 L_p \|\mu\|_{L^\infty(\Gamma_C)} \|\boldsymbol{u}^n - \boldsymbol{u}_I^n\|_V^2 \\
&\le c_0^2 L_p \|\mu\|_{L^\infty(\Gamma_C)} \|\boldsymbol{e}_h^n\|_V^2 + \epsilon_1 \|\boldsymbol{e}_h^n\|_V^2 + \frac{c_0^4 L_p^2 \|\mu\|_{L^\infty(\Gamma_C)}^2}{\epsilon_1} \|\boldsymbol{u}^n - \boldsymbol{u}_I^n\|_V^2 \\
&\quad + c_0^2 L_p \|\mu\|_{L^\infty(\Gamma_C)} \|\boldsymbol{u}^n - \boldsymbol{u}_I^n\|_V^2 \\
&\le (c_0^2 L_p \|\mu\|_{L^\infty(\Gamma_C)} + \epsilon_1) \|\boldsymbol{e}_h^n\|_V^2 + c \|\boldsymbol{u}^n - \boldsymbol{u}_I^n\|_V^2, \qquad (4.25)
\end{aligned}
$$

and

$$
\begin{aligned}
c \|\boldsymbol{u}^n - \boldsymbol{u}_h^n\|_V \|w^n - w_h^n\|_W &\le c \|\boldsymbol{e}_h^n\|_V \|w^n - w_h^n\|_W + c \|\boldsymbol{u}^n - \boldsymbol{u}_I^n\|_V \|w^n - w_h^n\|_W \\
&\le \epsilon_2 \|\boldsymbol{e}_h^n\|_V^2 + \frac{c^2}{4\epsilon_2} \|w^n - w_h^n\|_W^2 + \frac{c}{2} \|\boldsymbol{u}^n - \boldsymbol{u}_I^n\|_V^2 + \frac{c}{2} \|w^n - w_h^n\|_W^2 \\
&\le \epsilon_2 \|\boldsymbol{e}_h^n\|_V^2 + c \|\boldsymbol{u}^n - \boldsymbol{u}_I^n\|_V^2 + c \|w^n - w_h^n\|_W^2. \qquad (4.26)
\end{aligned}
$$

Due to the smallness condition $C_1 > c_0^2 L_p \|\mu\|_{L^\infty(\Gamma_C)}$, $A := C_1 - c_0^2 L_p \|\mu\|_{L^\infty(\Gamma_C)}$ is positive. We set $\epsilon_1 = \epsilon_2 = A/4$ and use (4.25)–(4.26) in (4.23) to obtain

$$
R_3 \le (c_0^2 L_p \|\mu\|_{L^\infty(\Gamma_C)} + \epsilon_1 + \epsilon_2) \|\boldsymbol{e}_h^n\|_V^2 + c \|\boldsymbol{u}^n - \boldsymbol{u}_I^n\|_V^2 + c \|\theta^n\|_W^2 + c \|\boldsymbol{u}^n - \boldsymbol{u}_I^n\|_{L^2(\Gamma_C)}. \qquad (4.27)
$$

Using (4.12), (4.13) and (4.27) in (4.11), combine the triangle inequality

$$
\begin{aligned}
\frac{A}{2} \|\boldsymbol{e}_h^n\|_V^2 &\le c \left(\|\boldsymbol{u}^n - \boldsymbol{u}_\pi^n\|_{V,h} + \|\boldsymbol{u}^n - \boldsymbol{u}_I^n\|_V + \|\boldsymbol{f} - \boldsymbol{f}_h\|_{V_h'} \right) \|\boldsymbol{e}_h^n\|_V \\
&\quad + c \|\boldsymbol{u}^n - \boldsymbol{u}_I^n\|_V^2 + c \|\theta^n\|_W^2 + c \|\boldsymbol{u}^n - \boldsymbol{u}_I^n\|_{L^2(\Gamma_C)}. \qquad (4.28)
\end{aligned}
$$

Applying the elementary result

$$
a, b, x \ge 0,\ x^2 \le ax + b \Rightarrow x^2 \le a^2 + 2b,
$$

we obtain

$$
\|\boldsymbol{e}_h^n\|_V^2 \le c \left(\|\boldsymbol{u}^n - \boldsymbol{u}_\pi^n\|_{V,h} + \|\boldsymbol{u}^n - \boldsymbol{u}_I^n\|_V + \|\boldsymbol{f} - \boldsymbol{f}_h\|_{V_h'} \right)^2 + c \|\theta^n\|_W^2 + c \|\boldsymbol{u}^n - \boldsymbol{u}_I^n\|_{L^2(\Gamma_C)}. \qquad (4.29)
$$

By the triangle inequality (4.24) and (4.7), we derive the result (4.6). ■

Combining the error estimate results of displacement and wear function, we have the following Ceá type inequality.

Theorem 4.6. *Under the assumptions stated in Theorem 3.4 and Assumption 4.4, we have the following error estimate:*

$$
\begin{aligned}
\max_{1 \le n \le N} \left(\|\boldsymbol{e}^n\|_V^2 + \|\theta^n\|_W^2 \right) &\le ck^2 + ck \|\boldsymbol{e}^0\|_V^2 + c \max_{1 \le n \le N} \|\boldsymbol{u}^n - \boldsymbol{u}_I^n\|_{L^2(\Gamma_C)} \\
&\quad + \max_{1 \le n \le N} c \left(\|\boldsymbol{u}^n - \boldsymbol{u}_\pi^n\|_{V,h} + \|\boldsymbol{u}^n - \boldsymbol{u}_I^n\|_V + \|\boldsymbol{f} - \boldsymbol{f}_h\|_{V_h'} \right)^2. \qquad (4.30)
\end{aligned}
$$

Proof. From (4.4) and (4.6),

$$
\begin{aligned}
\|\boldsymbol{e}^n\|_V^2 &\le c \left(\|\boldsymbol{u}^n - \boldsymbol{u}_\pi^n\|_{V,h} + \|\boldsymbol{u}^n - \boldsymbol{u}_I^n\|_V + \|\boldsymbol{f} - \boldsymbol{f}_h\|_{V_h'} \right)^2 + c \|\boldsymbol{u}^n - \boldsymbol{u}_I^n\|_{L^2(\Gamma_C)} \\
&\quad + ck^2 + c \sum_{m=0}^{n-1} k_m \left(\|\boldsymbol{e}^m\|_V^2 + \|\theta^m\|_W^2 \right). \qquad (4.31)
\end{aligned}
$$

Since $\theta^0 = w^0 - w_h^0 = 0$, add (4.4) and (4.31) together to get

$$
\begin{aligned}
\|\boldsymbol{e}^n\|_V^2 + \|\theta^n\|_W^2 &\le c \left(\|\boldsymbol{u}^n - \boldsymbol{u}_\pi^n\|_{V,h} + \|\boldsymbol{u}^n - \boldsymbol{u}_I^n\|_V + \|\boldsymbol{f} - \boldsymbol{f}_h\|_{V_h'} \right)^2 + c \|\boldsymbol{u}^n - \boldsymbol{u}_I^n\|_{L^2(\Gamma_C)} \\
&\quad + ck^2 + ck \|\boldsymbol{e}^0\|_V^2 + c \sum_{m=1}^{n-1} k_m \left(\|\boldsymbol{e}^m\|_V^2 + \|\theta^m\|_W^2 \right). \qquad (4.32)
\end{aligned}
$$

Applying Lemma 4.1, we derive the inequality (4.30) from (4.32). ■

We proceed to derive an optimal order error estimate for the fully discrete scheme.

Theorem 4.7. *Under the assumptions stated in Theorem 3.4 and Assumption 4.4, for the lowest order VEM with $k = 1$, we have the optimal order error estimate*

$$\max_{1\le n\le N} \left(\|e^n\|_V + \|\theta^n\|_W\right) \le c\,(k+h). \tag{4.33}$$

Proof. First, we bound the error $\|e^0\|_V$. By Lemma 4.5 and $\|\theta^0\|_W = 0$, we get

$$\|e^0\|_V^2 \le c\left(\|u^0 - u_\pi^0\|_{V,h} + \|u^0 - u_I^0\|_V + \|f - f_h\|_{V_h'}\right)^2 + c\|u^0 - u_I^0\|_{L^2(\Gamma_C)}. \tag{4.34}$$

For the lowest order VEM, by the approximation result in Proposition 3.1, for $n \in \{0, \cdots, N\}$, we have

$$\|u^n - u_\pi^n\|_{V,h} \le ch|u^n|_{2,\Omega}, \tag{4.35}$$

$$\|u^n - u_I^n\|_V \le ch|u^n|_{2,\Omega}, \tag{4.36}$$

$$\|u^n - u_I^n\|_{L^2(\Gamma_C)} \le ch^2\Big(\sum_{i=1}^{I} |u^n|^2_{2,\Gamma_{C,i}}\Big)^{1/2}. \tag{4.37}$$

In addition, using the approximation results in (3.16), we get

$$\|f_1 - f_{1h}\|_{V_h'} \le c\,h\,\|f_1\|_0. \tag{4.38}$$

By using Theorem 4.6 and putting (4.34)–(4.38) into (4.30), we obtain

$$\max_{1\le n\le N} \left(\|e^n\|_V^2 + \|\theta^n\|_W^2\right) \le ck^2 + ckh^2 + ch^2 \le c(k+h)^2.$$

Then we have the optimal-order error estimate (4.33). ■

Remark 4.8. It is known that for the numerical solution of a variational inequality, high-order finite elements do not lead to optimal order error estimates even if the solution is assumed to be smooth ([12]). Moreover, it is also known that the smoothness of the solution of a variational inequality is quite limited ([11]). For these reasons, it makes sense only to consider numerical methods with the lowest-order element ($k = 1$).

Remark 4.9. The term $\max_{1\le n\le N} \|u^n - u_I^n\|_{L^2(\Gamma_C)}$ in (4.30) represents an error occurring along the contact boundary. One strategy to reduce this error is to increase the degree of freedom along the contact boundary. As articulated in [36], we can do it by employing a locally refined mesh along the contact boundary. This approach is facilitated by the virtual element framework, wherein the incorporation of hanging nodes is permitted—a distinct advantage of VEM in tackling contact problems.

5. Numerical results

In this section, we report computer simulation results on some numerical experiments. Let $d = 2$ and consider a rectangular shaped set $\Omega = (0, 2) \times (0, 1)$ shown in Fig. 2 with the following partition of the boundary

$$\Gamma_D = \{0\} \times [0, 1], \quad \Gamma_N = ([0, 2] \times \{1\}) \cup (\{2\} \times [0, 1]), \quad \Gamma_C = [0, 2] \times \{0\}.$$

The linear elasticity operator $\mathcal{C}$ is defined by

$$\mathcal{C}(\tau) = 2\eta\,\tau + \lambda\,\mathrm{tr}(\tau)\mathcal{I}, \quad \tau \in \mathbb{S}^2,$$

where $\mathcal{I}$ denotes the identity matrix, tr denotes the trace of the matrix, $\lambda > 0$ and $\eta > 0$ are the Lamé coefficients. In our simulations, we select $\lambda = \eta = 4$, $T = 1$ and take the following dimensionless data:

$$\begin{aligned}
&u^0(x) = (0, 0), \quad x \in \Omega,\\
&p(r) = \begin{cases} 0.4r, & r \in [0, \infty),\\ 0, & r \in (-\infty, 0),\end{cases}\\
&f_1(x, t) = (0, -0.06), \quad x \in \Omega,\ t \in [0, T],\\
&f_2(x, t) = (0, 0), \quad x \in \Gamma_N,\ t \in [0, T],\\
&g = 0.1.
\end{aligned}$$

Remark 5.1. As λ tends towards infinity, many numerical methods for solving the linear elasticity system exhibit a locking phenomenon. In the literature, some locking-free virtual element methods have been developed. In [40], a nonconforming virtual element method for solving the linear elasticity problem is shown to uniformly converge with respect to the Lamé constant. A mixed virtual element method is introduced in [10] for solving near-incompressible linear elastic equations. A stress-hybrid virtual element method on quadrilateral meshes is proposed in [9] for compressible and nearly-incompressible linear elasticity.

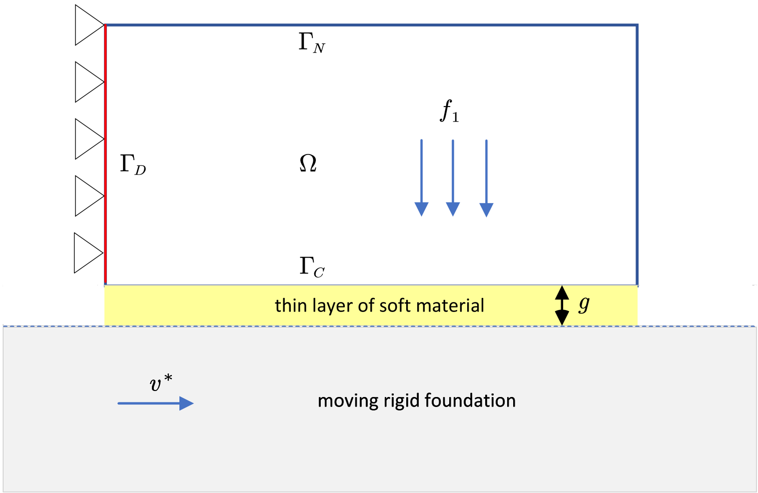

Fig. 2. Initial setting.

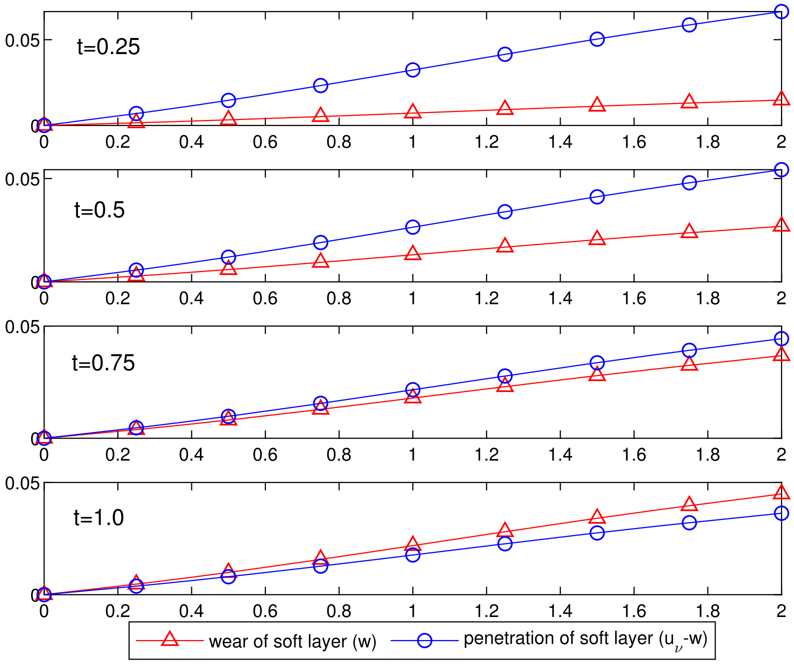

Fig. 3. Wear and penetration for $\mu = 0.2$, $\kappa = 2$, $\boldsymbol{v}^* = (1, 0)$ in Example 5.2.

We use the linear virtual element space V_h defined in (3.1) and its subset U_h defined in (3.4). To solve Problem 3.3, we use the Uzawa iteration described in [18] by introducing two Lagrange multipliers.

We first illustrate the impact of certain input data on the deformation of the body.

Example 5.2. In this example, we choose the following three data sets:

1. $\mu = 0.2, \kappa = 2, \boldsymbol{v}^* = (1, 0)$;
2. $\mu = 0.2, \kappa = 10, \boldsymbol{v}^* = (1, 0)$;
3. $\mu = 0.6, \kappa = 10, \boldsymbol{v}^* = (1, 0)$.

The numerical solutions correspond to the time step size $k = 1/64$, where the boundary Γ_C of the body is divided into 32 equal parts.

In all cases, we show the wear w and penetration $u_\nu - w$ of the soft layer of material covering Γ_C at $t = 0.25, 0.5, 0.75, 1$. Figs. 3–5 show corresponding graphs at these four moments. We observe a gradual increase of wear over time, which is consistent with our

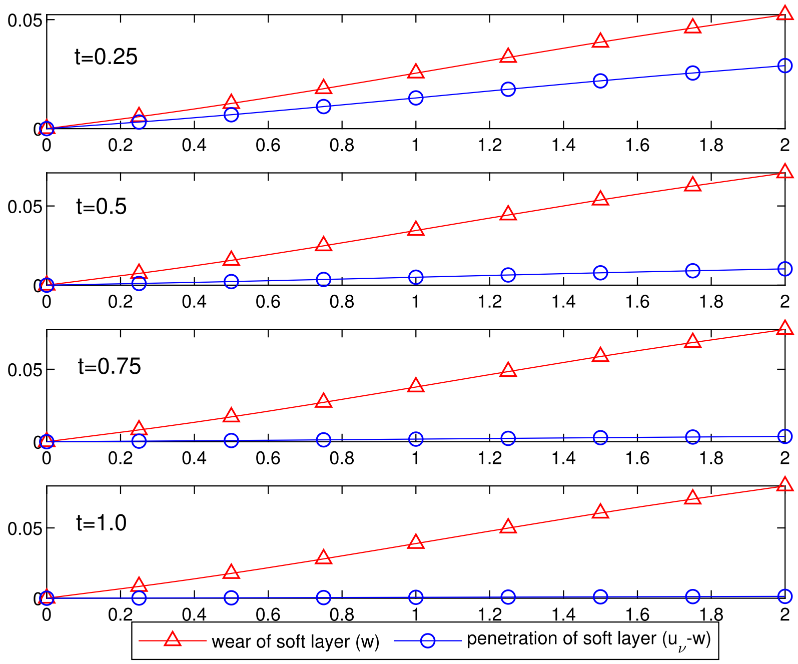

Fig. 4. Wear and penetration for $\mu = 0.2$, $\kappa = 10$, $\boldsymbol{v}^* = (1, 0)$ in Example 5.2.

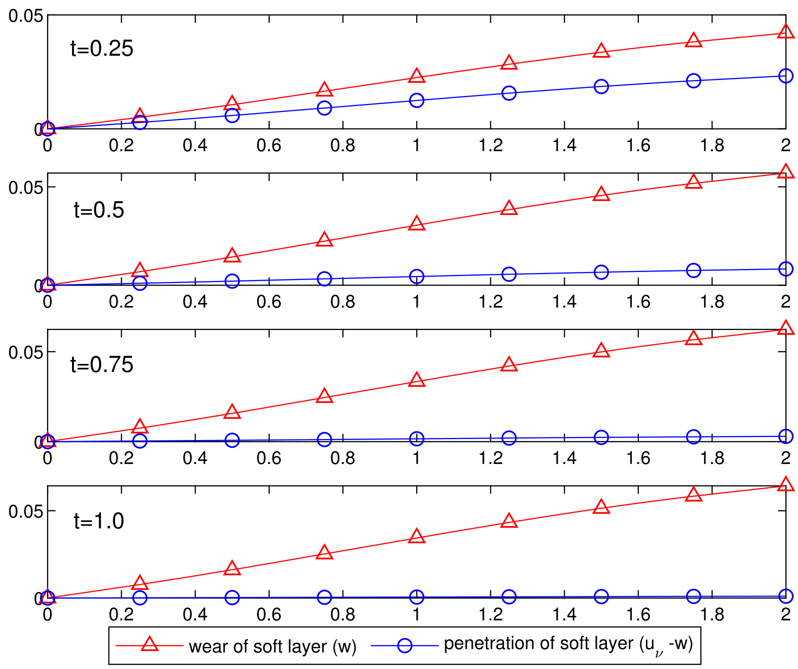

Fig. 5. Wear and penetration for $\mu = 0.6$, $\kappa = 10$, $\boldsymbol{v}^* = (1, 0)$ in Example 5.2.

daily life experience. Fig. 3 and Fig. 4 show that when we increase the wear coefficient κ from 2 to 10, the wear on the soft layer increases. Fig. 4 and Fig. 5 show that when we increase the friction coefficient μ from 0.2 to 0.6, the wear on the soft layer decreases, as a consequence of increased friction between the soft layer of material covering Γ_C and the rigid foundation.

Example 5.3. We report numerical results for four different time-step subdivisions, which are as follows:

1. Uniform partition with a time step of $k = 1/64$;
2. Non-uniform partition with $k_{2l-1} = 1/128$ and $k_{2l} = 3/128$ for $l = 1, 2, \dots$;

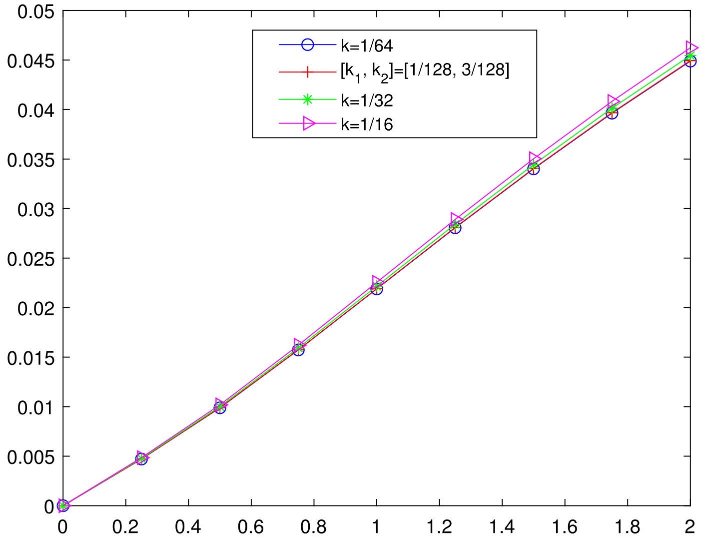

Fig. 6. Wear at $t = 1$ in Example 5.3.

3. Uniform partition with a time step of $k = 1/32$;
4. Uniform partition with a time step of $k = 1/16$.

In all cases, we study the wear on the soft layer for $t = 1$. In the simulation, we used a mesh size of $h = 1/16$, and the coefficients $\mu = 0.2$, $\kappa = 2$, $\boldsymbol{v}^* = (1, 0)$.

Fig. 6 shows the numerical solutions of the wear for the different time-interval partitions. It shows that for this example, the numerical solution for the non-uniform partition is similar to that for uniform partitions.

In order to verify the effectiveness of VEM on general polygonal meshes, we consider the following example:

Example 5.4. In space, we use the following two groups of grids:

1. Uniform mesh, the mesh size is $h = 1/32$, a total of 2048 squares;
2. General polygon mesh division, a total of 2048 polygons.

We compute the numerical solution of displacement $\boldsymbol{u}_h$ and the wear on the soft layer. In the simulation, time step-size $k = 1/64$, and the coefficients $\mu = 0.2$, $\kappa = 2$, $\boldsymbol{v}^* = (1, 0)$.

Fig. 7 and Fig. 8 show the numerical solutions of the displacement $\boldsymbol{u}_h = (u_{h1}, u_{h2})$ for the two meshes, respectively. We observe that the displacement u_{h1} and u_{h1} on these meshes are almost the same, which shows that the virtual element method works well on meshes. In addition, as shown in Fig. 9, we give the scatter plot of normal displacement on the contact boundary and the wear of the soft layer. It can be observed that the wear and normal displacement almost coincide at the same boundary position. At different locations, the two sets of scatter plots are almost smoothly connected and highly consistent, which further illustrates the effectiveness of VEM on general polygonal meshes.

Example 5.5. We use a uniform discretization of the problem domain and time interval according to the spatial discretization parameter h and time step k, respectively. The boundary Γ_C of Ω is divided into $2/h$ parts. We start with $h = 1/4$ and $k = 1/4$, which are successively halved. We give the relative error and error order of displacement and wear.

Since we do not know the true solution of the variational inequality, we use the numerical solution computed on a finer grid as the reference solution. In this example, we choose the numerical solution with $h = k = 1/256$ as the reference solution $\boldsymbol{u}_{ref}$ and w_{ref}. Because the virtual element solution $\boldsymbol{u}_h$ is not computable directly, we compute the relative error

$$\left\|\Pi_1(\boldsymbol{u}_h - \boldsymbol{u}_{ref})\right\|_{H^1} / \left\|\Pi_1 \boldsymbol{u}_{ref}\right\|_{H^1},$$

where the restriction of the projection Π_1 on K is defined by (3.8). In Table 1, we report the H^1 displacement error of the numerical solutions and the corresponding convergence orders. We observe that the numerical convergence orders are close to one, which matches well the theoretical prediction. For the wear function, we compute $\|w_h - w_{ref}\|_{L^2(\Gamma_C)}/\|w_{ref}\|_{L^2(\Gamma_C)}$. In Table 2, the numerical convergence orders for the numerical solutions of the wear function are also close to 1, which is consistent with theoretical analysis.

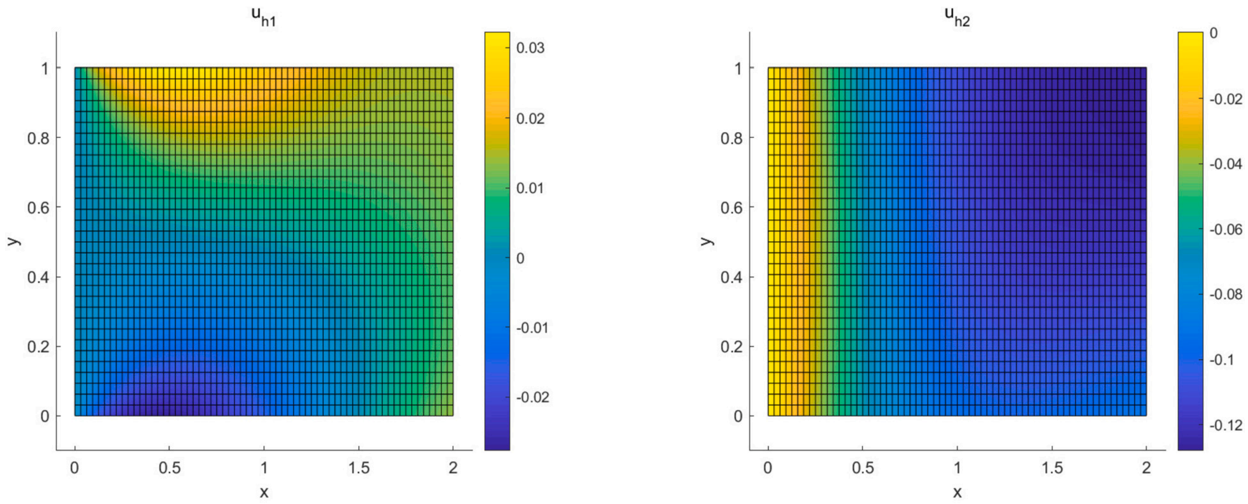

Fig. 7. Approximate solution for square mesh of $h = 2^{-5}$ in Example 5.4. (For interpretation of the colors in the figure(s), the reader is referred to the web version of this article.)

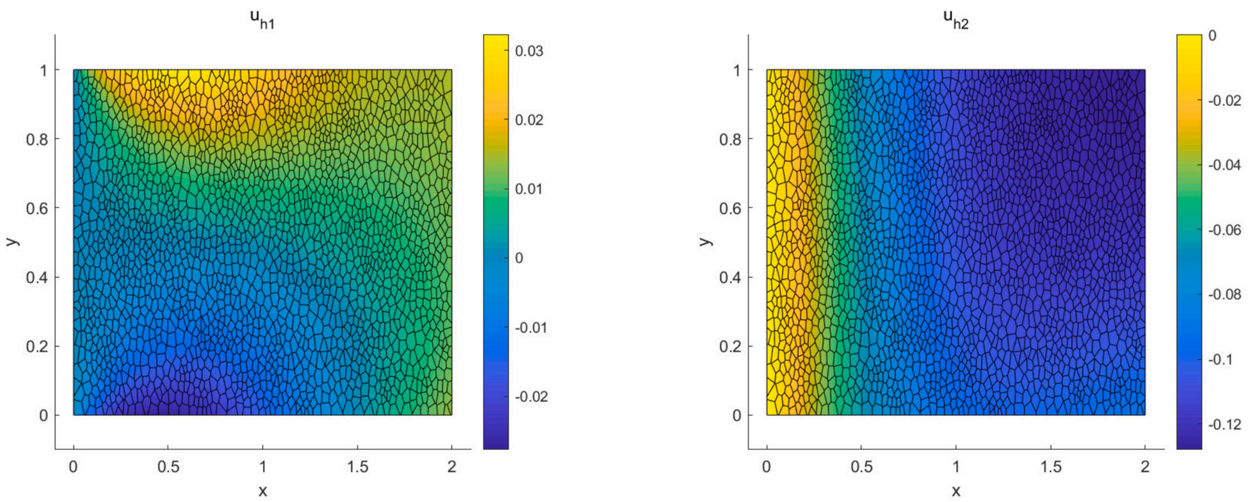

Fig. 8. Approximate solution for general polygon mesh of $h = 2^{-5}$ in Example 5.4.

Table 1
Numerical error for displacement in Example 5.5.

$h = k$	2^{-2}	2^{-3}	2^{-4}	2^{-5}	2^{-6}
Error	7.0581e-2	3.9059e-2	2.1698e-2	1.2084e-2	6.5023e-3
Order	-	0.85365	0.84807	0.84448	0.89407

Table 2
Numerical error for wear in Example 5.5.

$h = k$	2^{-2}	2^{-3}	2^{-4}	2^{-5}	2^{-6}
Error	1.1153e-1	5.4917e-2	2.5228e-2	1.1795e-2	5.4869e-3
Order	-	1.0221	1.1223	1.0968	1.1041

CRediT authorship contribution statement

Bangmin Wu: Data curation, Formal analysis, Methodology, Software, Visualization, Writing – original draft. **Fei Wang:** Conceptualization, Formal analysis, Investigation, Project administration, Resources, Supervision, Writing – original draft, Writing – review & editing. **Weimin Han:** Conceptualization, Formal analysis, Supervision, Writing – original draft, Writing – review & editing.

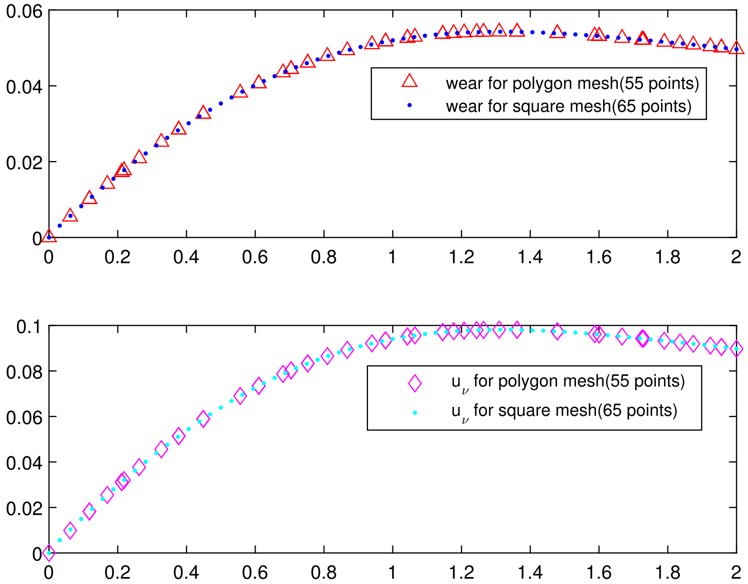

Fig. 9. Wear w and the normal displacement u_ν in Example 5.4.

Acknowledgement

The work of the first author was partially supported by Talent Project of the Tianchi Doctoral Program in Xinjiang Uygur Autonomous Region (Grant No. 5105240152n), Natural Science Foundation of Xinjiang Uygur Autonomous Region (Grant No. 2023D14014) and Science and Technology Innovation Team Project (No. 2022TSYCTD0019). The work of the second author was partially supported by the National Natural Science Foundation of China (Grant No. 12171383) and Shaanxi Fundamental Science Research Project for Mathematics and Physics (Grant No. 22JSY027). The work of the third author was partially supported by Simons Foundation Collaboration, USA, Grant No. 850737.

References

[1] P.F. Antonietti, L. Beirão da Veiga, S. Scacchi, M. Verani, A C^1 virtual element method for the Cahn-Hilliard equation with polygonal meshes, SIAM J. Numer. Anal. 54 (2016) 34–56.
[2] M.F. Benedetto, S. Berrone, A. Borio, S. Pieraccini, S. Scialo, Order preserving SUPG stabilization for the virtual element formulation of advection-diffusion problems, Comput. Methods Appl. Mech. Eng. 311 (2016) 18–40.
[3] L. Beirão da Veiga, F. Brezzi, A. Cangiani, G. Manzini, L.D. Marini, A. Russo, Basic principles of virtual element methods, Math. Models Methods Appl. Sci. 23 (2013) 119–214.
[4] L. Beirão da Veiga, F. Brezzi, L.D. Marini, Virtual elements for linear elasticity problems, SIAM J. Numer. Anal. 51 (2013) 794–812.
[5] L. Beirão da Veiga, C. Lovadina, A. Russo, Stability analysis for the virtual element method, Math. Models Methods Appl. Sci. 27 (2017) 2557–2594.
[6] L. Beirão da Veiga, C. Lovadina, G. Vacca, Virtual elements for the Navier-Stokes problem on polygonal meshes, SIAM J. Numer. Anal. 56 (2018) 1210–1242.
[7] S.C. Brenner, L.R. Scott, The Mathematical Theory of Finite Element Methods, third edition, Springer-Verlag, New York, 2008.
[8] J. Chen, W. Han, M. Sofonea, Numerical analysis of a quasistatic problem of sliding frictional contact with wear, Methods Appl. Anal. 7 (2000) 687–704.
[9] A. Chen, N. Sukumar, Stress-hybrid virtual element method on quadrilateral meshes for compressible and nearly-incompressible linear elasticity, Int. J. Numer. Methods Eng. 125 (3) (2024) e7384.
[10] H. Duan, Z. Li, A mixed virtual element method for nearly incompressible linear elasticity equations, Adv. Comput. Math. 49 (2023) 11.
[11] P.G. Ciarlet, The Finite Element Method for Elliptic Problems, North-Holland, Amsterdam, 1978.
[12] R.S. Falk, Error estimates for the approximation of a class of variational inequalities, Math. Comput. 28 (1974) 963–971.
[13] F. Feng, W. Han, J. Huang, Virtual element methods for elliptic variational inequalities of the second kind, J. Sci. Comput. 80 (2019) 60–80.
[14] F. Feng, W. Han, J. Huang, Virtual element method for an elliptic hemivariational inequality with applications to contact mechanics, J. Sci. Comput. 81 (2019) 2388–2412.
[15] F. Feng, W. Han, J. Huang, Virtual element method for elliptic hemivariational inequalities with a convex constraint, Numer. Math., Theory Methods Appl. 14 (2021) 589–612.
[16] L. Gasinski, A. Ochal, M. Shillor, Quasistatic thermoviscoelastic problem with normal compliance, multivalued friction and wear diffusion, Nonlinear Anal., Real World Appl. 27 (2016) 183–202.
[17] A.L. Gain, C. Talischi, G.H. Paulino, On the virtual element method for three-dimensional elasticity problems on arbitrary polyhedral meshes, Comput. Methods Appl. Mech. Eng. 282 (2014) 132–160.
[18] R. Glowinski, Numerical Methods for Nonlinear Variational Problems, Springer-Verlag, New York, 1984.
[19] D. Han, W. Han, M. Jureczka, A. Ochal, Numerical analysis of a contact problem with wear, Comput. Math. Appl. 79 (2020) 2942–2951.
[20] W. Han, On the numerical approximation of a frictional contact problem with normal compliance, Numer. Funct. Anal. Optim. 17 (1996) 307–321.
[21] W. Han, M. Shillor, M. Sofonea, Variational and numerical analysis of a quasistatic viscoelastic problem with normal compliance, friction and damage, J. Comput. Appl. Math. 137 (2001) 377–398.
[22] W. Han, M. Sofonea, Quasistatic Contact Problems in Viscoelasticity and Viscoplasticity, American Mathematical Soc., 2002.
[23] W. Han, M. Sofonea, Numerical analysis of hemivariational inequalities in contact mechanics, Acta Numer. 28 (2019) 175–286.

[24] M. Jureczka, A. Ochal, Numerical analysis and simulations of contact problem with wear, Comput. Math. Appl. 77 (2019) 2980–2988.
[25] K.L. Kuttler, M. Shillor, Dynamic contact normal compliance wear and discontinuous friction coefficient, SIAM J. Math. Anal. 34 (2002) 1–27.
[26] C.Y. Lee, J.T. Oden, A priori error estimation of *hp*-finite element approximations of frictional contact problems with normal compliance, Int. J. Eng. Sci. 31 (1993) 927–952.
[27] I. Perugia, P. Pietra, A. Russo, A plane wave virtual element method for the Helmholtz problem, ESAIM: M2AN 50 (2016) 783–808.
[28] M. Sofonea, A. Matei, Mathematical Models in Contact Mechanics, Cambridge University Press, 2012.
[29] M. Sofonea, F. Pătrulescu, Y. Souleiman, Analysis of a contact problem with wear and unilateral constraint, Appl. Anal. 95 (2016) 2590–2607.
[30] J.M. Viaño, Á. Rodríguez-Arós, M. Sofonea, Asymptotic derivation of quasistatic frictional contact models with wear for elastic rods, J. Math. Anal. Appl. 401 (2013) 641–653.
[31] P. Wriggers, W.T. Rust, B.D. Reddy, A virtual element method for contact, Comput. Mech. 58 (2016) 1039–1050.
[32] F. Wang, B.D. Reddy, A priori error analysis of virtual element method for contact problem, Fixed Point Theory Algorithms Sci. Eng. 2022 (2022) 10.
[33] F. Wang, S. Shah, W. Xiao, A priori error estimates of discontinuous Galerkin methods for a quasi-variational inequality, BIT Numer. Math. 61 (2021) 1005–1022.
[34] F. Wang, H. Wei, Virtual element method for simplified friction problem, Appl. Math. Lett. 85 (2018) 125–131.
[35] F. Wang, H. Wei, Virtual element methods for obstacle problem, IMA J. Numer. Anal. 40 (2020) 708–728.
[36] F. Wang, B. Wu, W. Han, The virtual element method for general elliptic hemivariational inequalities, J. Comput. Appl. Math. 389 (2021) 113330.
[37] B. Wu, F. Wang, W. Han, Virtual element method for a frictional contact problem with normal compliance, Commun. Nonlinear Sci. Numer. Simul. 107 (2022) 106125.
[38] W. Xiao, F. Wang, W. Han, Discontinuous Galerkin methods for solving a frictional contact problem with normal compliance, Numer. Funct. Anal. Optim. 39 (2018) 1248–1264.
[39] J. Zhao, S. Chen, B. Zhang, The nonconforming virtual element method for plate bending problems, Math. Models Methods Appl. Sci. 26 (2016) 1671–1687.
[40] B. Zhang, J. Zhao, Y. Yang, S. Chen, The nonconforming virtual element method for elasticity problems, J. Comput. Phys. 378 (2019) 394–410.